Manganese in South Africa: its mineral economics, geology and geometallurgy

B.P. von der Heyden
African Rainbow Minerals Chair in Geometallurgy, Department of Earth Sciences, Stellenbosch University, Private Bag X1, Matieland 7602, South Africa
Department of Science and Innovation – National Research Foundation Centre of Excellence for Integrated Mineral and Energy Resource Analysis, Department of Geology, University of Johannesburg, P.O. Box 524, Auckland Park, 2006, Johannesburg, South Africa
e-mail: bvon@sun.ac.za

A.J.B. Smith
Department of Science and Innovation – National Research Foundation Centre of Excellence for Integrated Mineral and Energy Resource Analysis, Department of Geology, University of Johannesburg, P.O. Box 524, Auckland Park, 2006, Johannesburg, South Africa
Paleoproterozoic Mineralisation Research Group, Department of Geology, University of Johannesburg, P.O. Box 524, Auckland Park, 2006, Johannesburg, South Africa
e-mail: bertuss@uj.ac.za

H. Tsikos
Department of Earth Sciences, Stellenbosch University, Private Bag X1, Matieland 7602, South Africa
Department of Geology, University of Patras, Rion 26504, Patras, Greece
e-mail: htsikos@upatras.gr

M. Tadie
African Rainbow Minerals Chair in Geometallurgy, Department of Process Engineering, Stellenbosch University, Private Bag X1, Matieland 7602, South Africa
e-mail: mtadie@sun.ac.za

X. Mhlanga
School of Biology and Environmental Sciences, Faculty of Agriculture and Natural Sciences, University of Mpumalanga, Cnr R40 and D725 Road, Mbombela, South Africa
e-mail: xolane.mhlanga@ump.ac.za

L. van Eeden
African Rainbow Minerals Chair in Geometallurgy, Department of Earth Sciences, Stellenbosch University, Private Bag X1, Matieland 7602, South Africa
e-mail: 22664580@sun.ac.za

N. Backeberg
Department of Earth Sciences, Stellenbosch University, Private Bag X1, Matieland 7602, South Africa
The Project Blue Group Limited, 71-75 Shelton Street, Covent Garden, London, WC2H 9JQ, United Kingdom
e-mail: nils@projectblue.com

T.G. Schultz
The Project Blue Group Limited, 71-75 Shelton Street, Covent Garden, London, WC2H 9JQ, United Kingdom
e-mail: tanisha.schultz@projectblue.com

C. Djeutchou
African Rainbow Minerals Chair in Geometallurgy, Department of Earth Sciences, Stellenbosch University, Private Bag X1, Matieland 7602, South Africa
e-mail: djeutchoucdric@gmail.com

Abstract

Manganese (Mn) is a crucial metal for steelmaking and is increasingly being sought after for its use in the battery and clean-energy sectors. Through discovery of the Kalahari Manganese Field (KMF), the world's largest land-based Mn resource, South Africa has positioned itself as a major player in the global Mn supply chain. However, only a fraction of this total Mn resource is currently being exploited, and opportunities for further exploitation in the KMF and at several other Mn deposits and occurrences throughout South Africa remain to be realised. To consolidate scientific and industrial interest in the entire South African Mn resource base, the present contribution provides a holistic overview of (1) global Mn mineral economics, (2) the processes that give rise to enrichment of Mn in crustal rocks, (3) the palaeoenvironmental implications of Mn enrichments, (4) the geology of domestic Mn deposits and occurrences, and (5) the geometallurgical and mineral processing paradigms applicable to full value realisation from these diverse ore types. South African Mn deposits are broadly subdivided into those formed from chemical sedimentary processes and subsequent diagenesis (e.g., the KMF, deep-sea Mn nodules and crusts); those formed as residual enrichments after chemical weathering of Mn-bearing protolith (e.g., North West Manganese Fields); and those formed through mobilisation by hydrothermal fluids and groundwater (e.g., vein and breccia-hosted deposits in fractured lithologies in the Cape Supergroup, Waterberg Group, etc.). Because of these differences in the mechanisms of Mn deposit formation, and because of the various valence and ligand bonding interactions associated with Mn, the resultant mineralogy of the individual deposit groups is widely varied. Primary chemical sediments typically comprise Mn^{2+} carbonates, braunite and occasionally Mn^{2+} silicates, which may be locally upgraded to $Mn^{2+/3+}$ oxide minerals by subsequent hypogene enrichment. Low temperature deposits, including Mn nodules, groundwater-associated deposits, and residual accumulations are marked by Mn^{4+} mineral parageneses, which may subsequently be modified by regional metamorphism. Inasmuch as Mn grade is a primary variable governing economic Mn extraction, a growing body of geometallurgical work highlights that full value realisation will only be achieved through targeted exploitation of the Mn mineralogical diversity. This includes the realisation that Mn valence and ligand coordination impact the energy consumption and reagent utilisation during down-stream processing.

Introduction

Manganese (Mn) is a vital metal used in the production of essentially every tonne of steel, and as a key cathode material for the manufacture of modern lithium (Li) ion batteries. It is mainly produced in the Republic of South Africa (RSA; 36%), along with Gabon (23%), Australia (15%), Ghana (4.2%), China (3.7%), India (3.6%), and Brazil (3.1%) (Ziemann et al., 2013; Singh et al., 2020; USGS, 2024). There is a significant increase in demand for Mn alloys driven by the manufacturing industry which is, in turn, driven by rapid industrialisation of certain countries and by population growth. However, rapid depletion of high-grade Mn ore resources imposes challenges for Mn-based industries. These challenges are similar to those experienced in other commodity spaces and include the unavailability of high-grade raw materials, techno-economic difficulties associated with beneficiation of low-grade ores, and environmental restriction on ore processing technologies (e.g., CO_2 emission and toxic waste disposal; Lund, 2013; Aasly and Ellefmo, 2014; Ortiz, 2019; Singh et al., 2020; Gholami et al., 2022; Chetty et al., 2023). Manganese is increasingly listed on governments' critical materials lists, appearing in over half of the lists evaluated in a review by McNulty and Jowitt (2021). These lists highlight the economic importance of a metal in a context of the intrinsic risks associated with its supply chain.

Because of these issues, and because of South Africa's positioning as a major supplier to global mining outputs and as a major resource and reserve base (USGS, 2024), a review of the local Mn geology and its geometallurgy is both timely and geographically relevant. Scientific understanding of South Africa's world-class endowment of this critical metal is well-advanced, with comprehensive reviews provided by Cairncross et al. (1997), Astrup and Tsikos (1998), Cairncross and Beukes (2013), and Beukes et al. (2016). Renewed interest in Mn,

facilitated in part by the evolving transition to green metals for responsible metal production, warrants an update to these works. The present contribution thus encompasses a brief introduction to the current status of Mn mineral economics, an introduction to Mn mineralogy and nomenclature, before describing the various mechanisms by which Mn has become enriched in near-surface rocks within South Africa. This is followed by a descriptive review of a number of South African world-class and minor Mn mineral deposits (Figure 1) with emphasis on geology and mineralogy. As may be expected for an element that has three different valence states in the natural environment (Mn^{2+}, Mn^{3+} and Mn^{4+}), and which readily binds with a variety of ligand groups (oxides, carbonates, silicates, etc.), the observed mineralogy in the various deposits reviewed is highly diverse. Given that this mineralogical (and textural) diversity exists between deposits, we underline the importance of developing detailed understanding of these differences to advise targeted exploration and optimised mining and beneficiation approaches. These differences can also be exploited using geometallurgical paradigms to ensure that environmentally sustainable, economically viable and efficient production processes are developed for each of the diverse Mn deposits, thus ensuring efficient and responsible value realisation from South Africa's Mn resource base.

Manganese mineral economics

Human civilisation has found use for Mn for centuries, with some of its earliest applications being as pigments in cave paintings during the Stone Age and as a decolouriser or as a pink-purple pigment in ancient Roman and Egyptian glassware (Corathers, 2005). Manganese's dominance in steelmaking, where over 90% of its production is utilised (Westfall et al., 2016), underlines its economic significance. However, Mn faces

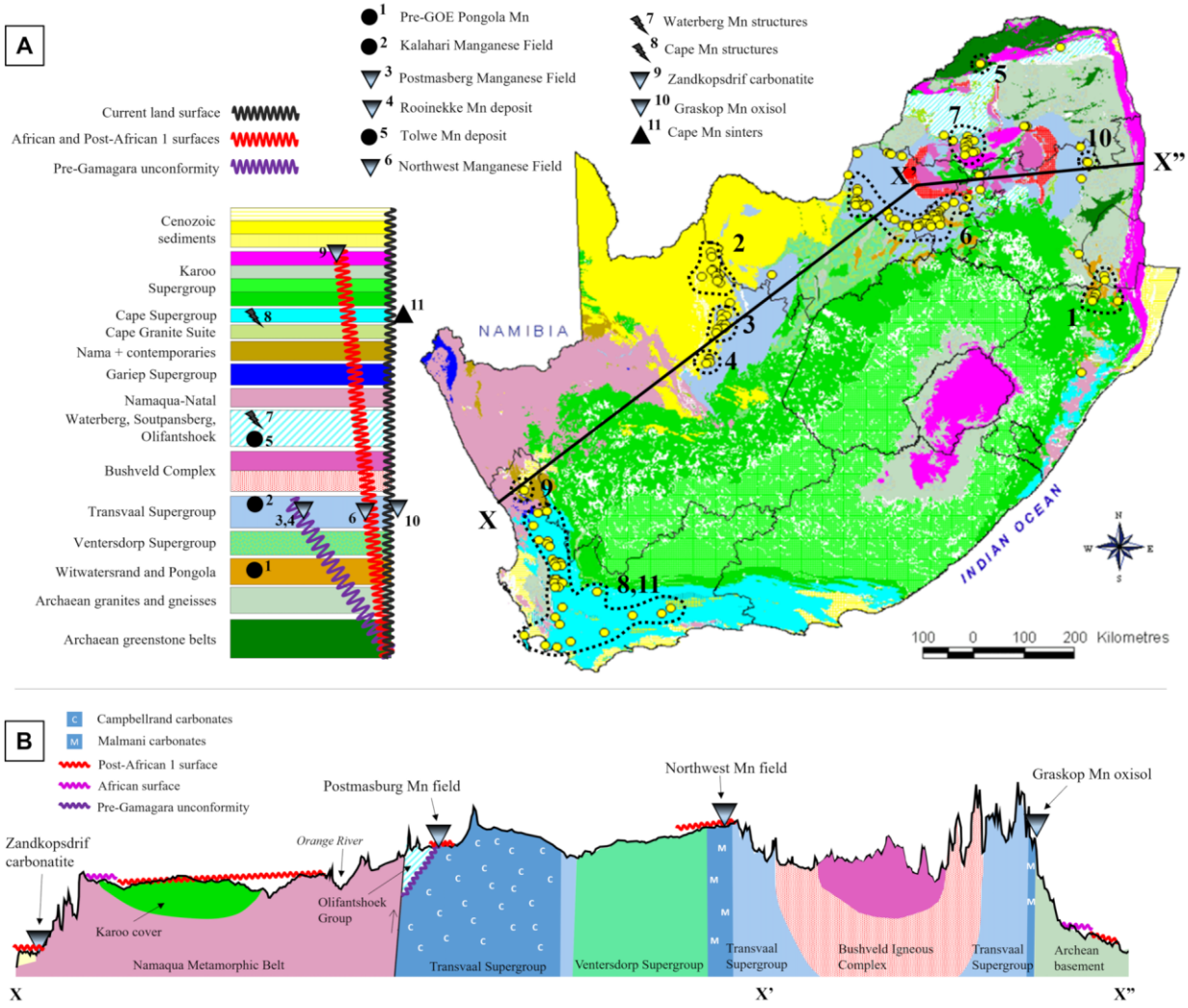

Figure 1. *(**A**) Temporal and spatial locations of all South African manganese (Mn) deposits documented or alluded to in this contribution. Background Mn distribution map taken from the Council of Geoscience (https://www.geoscience.org.za/cgs/systems/publications/downloadable-material/; accessed June 2023). (**B**) Transect X-X'-X" showing the inter-relationship between various unconformity surfaces and the development of several of the notable Mn accumulations that are detailed in the main text. Vertical exaggeration is approximately 140x.*

growing challenges due to the depletion of high-grade ores and the environmental concerns associated with mining and processing (Aasly and Ellefmo, 2014; Chetty et al., 2023). These factors not only elevate the cost of extraction but also increase reliance on lower-grade ores, posing further techno-economic hurdles. Moreover, global demand continues to rise particularly from rapidly industrialising nations, thus necessitating that a sustainable and diversified supply chain is ensured to prevent future bottlenecks.

Drivers of manganese demand

Since the mid-90s, significant advancements have been made in high-strength low-alloy (HSLA) steels. Many of these advancements arise from optimising the ratios of the respective alloying elements (e.g., Mn) which allows for a favourable balance of strength, low-temperature toughness, ductility, weldability, a simplified production process, and cost-effectiveness (Aleksandrov et al., 2005). Manganese is primarily used in the form of alloys (FeMn, SiMn, AlMn, etc.), pure metal oxides (MnO, Ɣ-MnO_2, etc.) and numerous other Mn compounds ($KMnO_4$, $MnCl_2$, $MnSO_4$). For the steel industry, Mn is typically added as either ferromanganese (FeMn) or ferro-silicomanganese (SiMn; Figure 2) (Singh et al., 2020). Ferro- silicomanganese has captured more market share than FeMn (mostly in China and India), as steel makers can benefit from the additional silicon which, like Mn, is required in the steelmaking process. Ore feed qualities are a crucial consideration for the steel-making industry. For example, Mn ores may contain deleterious elements such as phosphorus (P), which reduces the toughness of steel. The ratio of phosphorus to manganese (Mn/P) is a critical parameter in the production of high-carbon ferromanganese (HC FeMn), as well as in silicomanganese processes, though to a lesser extent. This ratio is essential for maintaining the quality of the final metal product, as excessive phosphorus can negatively affect the mechanical properties of steel. Ores with a high Mn/P ratio, such as those from Gabon's Comilog mine, are highly sought after due to their ability to meet stringent global specifications for ferroalloys (Bao et al., 2024). In addition to Mn/P, the iron-to-manganese ratio (Mn/Fe) is another key factor in fine-tuning the composition of the final ferroalloy (Table 1). A higher Mn/Fe ratio enhances the control over the Mn content in the production process, improving overall metallurgical efficiency and product quality (Pochart et al., 2007; Kivinen et al., 2010). This ability to optimise both Mn/P and Mn/Fe ratios through the blending of ores from various sources makes certain ores, such as South African ores, highly competitive in the global market for ferroalloy production (Visser et al., 2013). Overall, high-grade ores are capable of improving cost competition in alloy making and carbonate

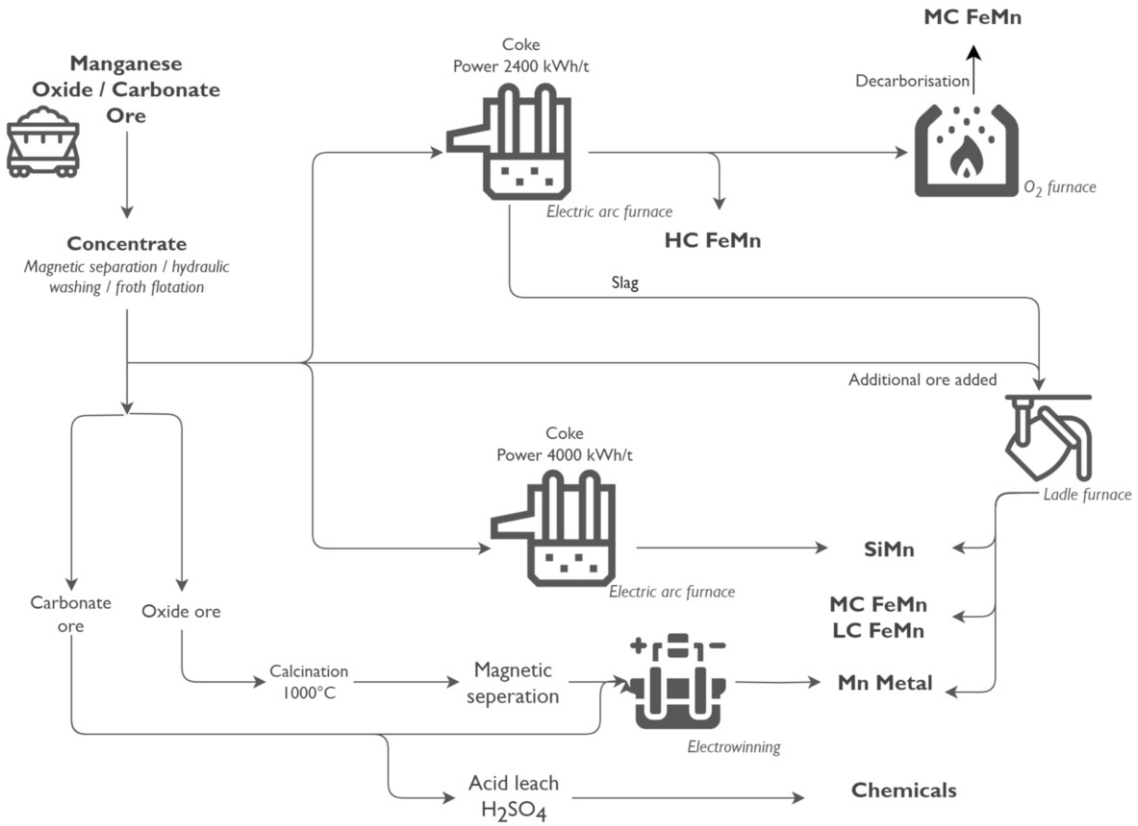

Figure 2. *A schematic overview of the most important manganese (Mn) beneficiation pathways in which Mn ores are used as feed to produce High Carbon Ferromanganese (HC FeMn), Medium Carbon Ferromanganese (MC FeMn) and silicomanganese (SiMn) for the steel sector, and Mn chemicals which are commonly used in the battery sector.*

Table 1. Synthesis of the 2022 data for grade, production data and ore types associated with manganese (Mn) mining operations in South Africa. Data collated by Project Blue and further references are available upon request.

Manganese field*	Status	Mine	Operator	Grade	Ore type**	Fe/Mn	2022 Production (kt)
W-PMF	Operating	Boskop Mine	DVD Mining	35%	Fe-Mn ore	-	295
W-PMF	Operating	Bishop Mine	PMG Mining	34%	Fe-Mn ore	-	738
W-PMF	Operating	Kitso Mine (Prev. Lohatlha)	Kitso Mining/Misty Falls	37%	Fe-Mn ore	-	590
W-PMF	Operating	Lomoteng Mine	Huatian SA mining and investment	26%	Fe-Mn ore	-	98
E-PMF	Operating	Salene Mine	Salene Manganese	35%	Si-Mn ore	-	295
W-PMF	Operating	Paling Mine	PMG Mining	35%	Fe-Mn ore	1.35	738
W-PMF	Operating	Glosam manganese	Emang Mmogo Mining Resources	32%	Fe-Mn ore	-	148
E-PMF	Operating	Morokwa Mine	Afrimat	35%	Si-Mn ore	-	98
PMF	Idle	Kareepan	Misty Falls	37%	Fe-Mn ore	-	-
E-PMF	Project	Pensfontein	Cape 26	-	Si-Mn ore	-	-
KMF	Operating	Nchwaning	African Rainbow Minerals	43%	Oxide	2.72	3 170
KMF	Operating	Tshipi	Tshipi é Ntle Manganese Mining	34%	Oxide	6.7 (5)	3 796
KMF	Operating	UMK	United Manganese of Kalahari	35%	Oxide	5.75 (3)	3 000
KMF	Operating	Wessels	South 32	48%	Oxide	4.38 (4)	419
KMF	Operating	Kudumane	Kudumane Manganese Resources	35%	Semi-carbonate	-	1 800
KMF	Operating	Kalagadi	Kalagadi Manganese	35%	Semi-carbonate	-	1 300
KMF	Operating	Mokala	Glencore	35%	Semi-carbonate	-	1 100
KMF	Operating	Gloria	African Rainbow Minerals	37%	Semi-carbonate	5.9 (1)	980
KMF	Operating	Mamatwan	Hotazel Manganese Mines	40%	Semi-carbonate	8.5 (2)	1 604
KMF	Project	Mn48 (prev Lehateng)	Mn48	48%	Oxide	-	-
KMF	Operating	Perth Mine	Sebilo Resources	35%	Semi-carbonate	-	500
KMF	Operating	East Manganese	Sitatunga Resources	35%	Semi-carbonate	-	200
NWMF	Closed	Manganese Minerals	New Venture Mining Resources (prev. Metmin)	30%	Semi-carbonate	0.43 (1)	-
NWMF	Operating	Innovage Resources	Artika	36%		-	800
NWMF	Operating	General Nice Manganese Mine	General Nice Manganese	15%	Mn wad/nodules	-	-

*Acronyms: KMF: Kalahari Manganese Fields; W-PMF: Western Postmasburg Manganese Fields; E-PMF: Eastern Postamasburg Manganese Fields; NWMF: North West Manganese Fields
**Ore types classification is after Bussin (2022). 'Semi-carbonate' is a term describing carbonate-rich Mn ores that contain variable amounts of other minerals e.g., oxides.

References: (1) Sundqvist et al. 2017; (2) Markgraaff, 2019; (3) Davies et al., 2023; (4) Anacleto et al., 2004; (5) Kozak, 2019; Additional information from published company Resource and Reserve Reports.

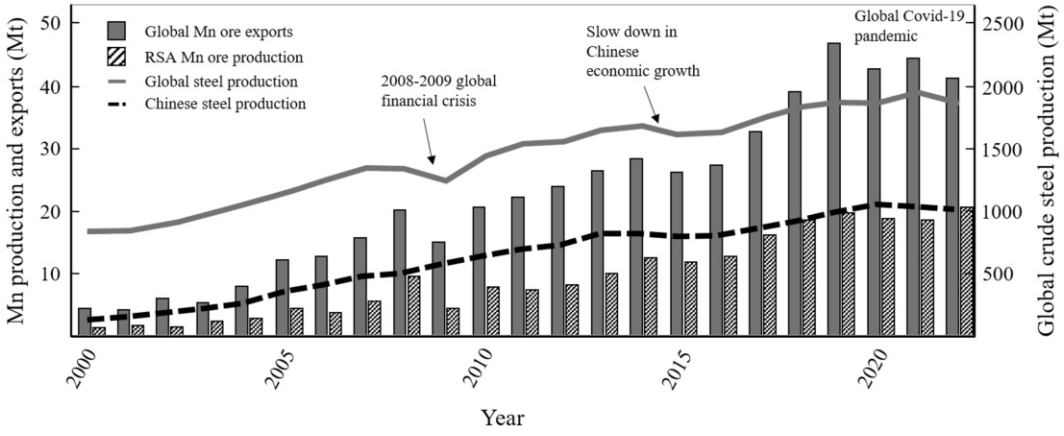

Figure 3. *Global crude steel production growth has increased over the last two decades, based largely on growth in production out of China (World Steel Association (worldsteel.org)), which accounts for over half of annual output. Manganese (Mn) production has followed suit, with most of the supply coming from South Africa and headed for the export market (data adapted from UN Comtrade (comtrade.un.org)) for conversion to alloys in China. Data collated by Project Blue and is available upon request.*

varieties offer energy saving during sintering (Figure 2) (e.g., Steenkamp et al., 2020).

The steel industry – and by extension Mn – has gone through two decades of restructuring in line with society's accelerated economic growth, particularly in China (Figure 3). There have been three key events impacting the overall global steel supply-demand-price dynamics (Figure 3). The first was the 2008/09 global financial crisis, following which China's annual economic growth rate slowed significantly (Long et al., 2016). This in turn resulted in the price of steel products reaching lows in 2015 and 2016, which added significant pressure to industrial restructuring within the steel sector (Long et al., 2016). The most recent disruptor was the COVID-19 pandemic, which had profound pricing impacts across a broad array of commodities. Recently, Mn is attracting new attention for its use in Li-ion batteries, due to its high theoretical specific capacity, safety, environmental friendliness and low cost (Bao et al., 2024; Gao et al., 2024). The battery industry is the largest market for non-alloy Mn, accounting for 3% of Mn consumption worldwide (Naseri et al., 2022). Manganese in batteries is a different supply chain to its traditional ferroalloy-steel route, with battery-makers using high-purity Mn sulphate as the main feedstock (Figure 2). From a consumer market perspective, low-grade ores have become a suitable feedstock for battery applications, with the most common feed being oxide ores. Other uses of Mn are minor but may be of local importance. These include its use as pigments (e.g., in bricks), in the chemicals sector, animal feed and in fertilisers (Steenkamp et al., 2020; USGS, 2024).

The South African manganese supply chain

The first mine to open in the Kalahari Manganese Field (KMF) was the Black Rock mine in 1940, followed in quick succession by the Devon and Smartt mines in 1954 and 1959 respectively, and by the large opencast Mamatwan mine in 1963 (Cape Minerals, 2017). Following the installation of a private railway by Assmang in the 1970's, the Gloria, Belgravia, Wessels and N'Chwaning I mines opened. More recently, the N'Chwaning II opened in 2004 and the N'Chwaning III opened in 2006. The Smartt mine was also reopened in 2008 due to ongoing development and expansion within the KMF (Cairncross and Beukes, 2013). Several other large and new operations in the KMF include Tshipi Borwa, United Manganese of Kalahari (UMK), Kalagadi and Kudumane. The Postmasburg Manganese Field (PMF) has also seen an increase in mining activity recently, with 12 active mines situated around the town of Postmasburg. Although many of these mines target iron ore (derived from chemical sedimentary protolith and intimately associated with Mn), several are Mn operations (e.g., Boskop, Glosam, among others; Cairncross, 2024) associated with palaeo-karstic environments (Gutzmer and Beukes, 1996a) and possible hydrothermal fluid flow (Fairey et al., 2019).

South Africa is the largest single supplier of Mn in the world, accounting for ~36% of the world's 2022 annual production, ~38% of all known global Mn reserves (Figure 3; USGS, 2024), and more than 77% of the world's land-based Mn resources (Beukes et al., 2016). Most of the South African Mn supply derives from the world-class KMF which comprises a diverse mineralogy containing oxide-, carbonate- and mixed ore types with grades varying from low to high-grade (i.e., 27 to 45% Mn; Beukes et al., 2016; Table 1). Of the ore that is produced in the KMF, the export percentage has risen from 50% prior to 2005 to levels greater than 80% since 2013. This has largely been driven by the fast-growing demand for steel, due to the ongoing developments in China (Cairncross and Beukes, 2013). Despite the KMF offering ample Mn reserves and being cost-competitive, several challenges have hampered the optimal growth levels in the South African Mn sector. For example, South Africa used to be a leading ferroalloy producer because the production of energy-intensive Mn alloys benefited from low energy and labour costs (Steenkamp and Basson, 2013). However, with rising energy costs and insecure supply, the domestic ferroalloy sector has diminished. Logistical issues remain an ongoing

economic challenge for South African ore miners and traders. The KMF is remotely situated in the interior of the country with a minimum distance of ~850 km distance to any major port e.g., Durban, Coega, Gqeberha (Port Elizabeth), and Saldanha (Cairncross and Beukes, 2013). Transportation of the ore is inevitably an issue due to the high volumes of Mn that South Africa is producing, which means that ultimately six different harbours are used to export Mn (Christianson, 2024).

With the ongoing depletion of shallow, open-castable Mn resources, South Africa's underground mines are expected to play an increasingly significant role in determining the cost-based price of Mn. However, the ramping up of lower-cost deposits, such as Gabon's high-grade 44% Mn Moanda ore and Ghana's mid-grade 35% semi-carbonate ores, may put pressure on South African ore prices. Additionally, the projected closure of GEMCO, one of the world's largest Mn mines, by 2028 could further tighten global supply, potentially driving prices higher as other sources are relied upon to meet demand. The ongoing growth of the global steel industry and the large Mn resource base of the KMF will ensure that RSA remains an integral part of the global Mn supply chain. Despite this, a report published by South Africa's Council for Scientific and Industrial Research (CSIR) in April 2022 showed that current Mn mineral reserves have a depletion rate that will last less than 20 years (Khan et al., 2022), highlighting the importance of further exploration to convert more resources into reserves.

Brief overview of the common manganese ore minerals

Manganese has a 3d5 4s2 valence electron configuration which comprises seven valence electrons, and manifests as Mn occurring in the +II, +III and +IV valence states in most minerals. Because of its prevalence and variable valence, Mn is an essential constituent of over 250 minerals and is a trace element in several thousand other minerals where it incorporates as a minor substituent for essential structural ions such as Fe^{2+} and Mg^{2+} (Gilkes and McKenzie, 1998). Largely serving as an introduction to terminology and mineral nomenclature, we restrict our descriptions to the main ore minerals associated with Mn deposits and occurrences in RSA (Figures 1 and 4). For a more complete treatment of Mn mineralogy, the reader is referred to Dorr et al. (1973), Maynard (2003, 2010), Cairncross et al. (1997) and Cairncross and Beukes (2013).

Table 2 summarises the mineralogical properties of the main Mn ore minerals, which are broadly divided into oxide minerals common in supergene deposits, oxide minerals associated with hypogene enrichment, silica-bearing Mn minerals and carbonate minerals. Several of the minerals formed in low-temperature supergene biogeochemical environments are characterised by small grain sizes and may in some instances be quite poorly crystalline. For example, todorokite ($(Na,Ca,K)_2(Mn^{4+},Mn^{3+})_6O_{12}\bullet 4(H_2O)$), a hydrous mixed-valence Mn oxide with a tunnel crystallographic structure, is rather special in that it contains the largest-known tunnels, three by three octahedra wide (Cairncross and Beukes,

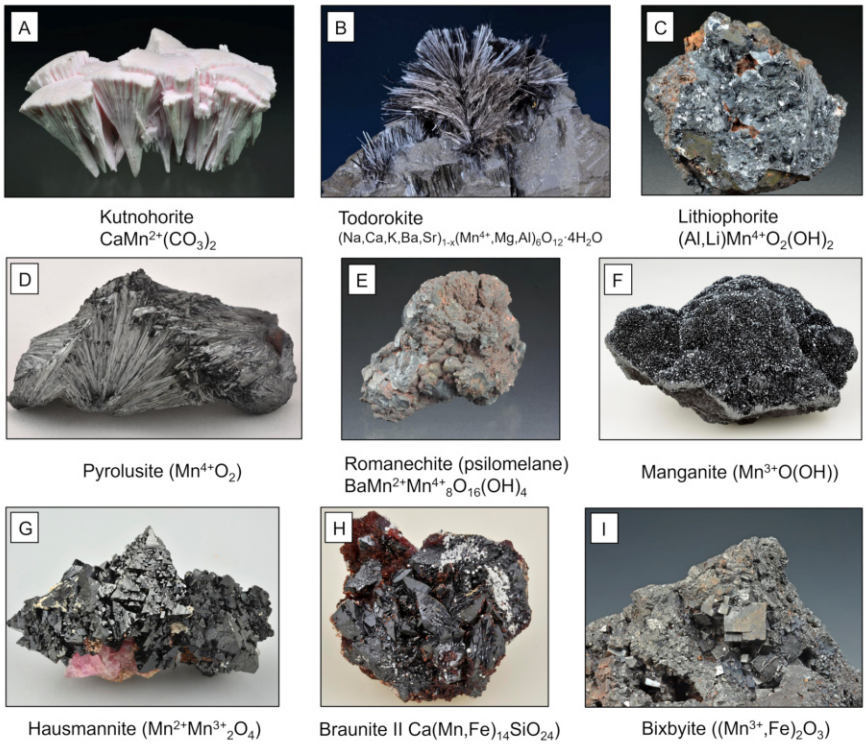

Figure 4. *Photographs of several important manganese (Mn) bearing minerals discussed in the text. All images kindly provided by Bruce Cairncross photographs. Sample sizes are respectively 12.8 cm (**A**); 4 cm (**B**); 9 cm (**C**); 4.3 cm (**D**); 9 cm (**E**); 11 cm (**F**); 5.2 cm (**G**); 5.2 cm ((**H**); associated with calcite and red andradite); and 2.1 cm (size of the field of view in (**I**)).*

Table 2. Selected properties for manganese (Mn) ore minerals mentioned in the text.

Grouping	Ore mineral	Formula	Valence	Density*	Magnetism*
Oxide ore *(commonly supergene alteration parageneses)*	Todorokite (10Å manganite)	$(Na,Ca,K,Ba,Sr)(Mn,Mg,Al)_6O_{12}{\cdot}3H_2O$	4+	3.66	Paramagnetic
	Birnessite (7Å manganite)	$Na_4(Mn_{14})O_{27}{\cdot}9H_2O$	4+	3	Paramagnetic
	Manganite	$MnO(OH)$	3+	4.32	
	Vernadite (disordered birnessite)	$(Mn,Fe,Ca,Na)(O,OH)_2 \cdot nH_2O$	4+	2.9	
	Cryptomelane	KMn_8O_{16}	4+; 3+	4.36	Paramagnetic
	Romanechite (psilomelane)	$(Ba,H_2O)_2Mn_5O_{10}$	4+; 3+	4.55	Paramagnetic
	Hollandite	$BaMn_8O_{16}$		4.95	
	Nsutite	$Mn(O,OH)_2$	4+; 2+	4.45	
	Lithiophorite	$(Al,Li)MnO_2(OH)_2$	4+	3.25	
	Pyrolusite	MnO_2	4+	4.73	Paramagnetic
Silicate and silica-bearing oxide ores	Braunite I	Mn_7SiO_{12}	3+; 2+	4.76	Ferromagnetic
	Braunite II	$Ca(Mn,Fe)_{14}SiO_{24}$	3+	4.72	Paramagnetic
	Friedelite	$Mn_8Si_6O_{15}(OH,Cl)_{10}$	2+	3.05	Ferromagnetic
Oxide ore (*upgraded*)	Hausmannite	Mn_3O_4	3+; 2+	4.76	Paramagnetic
	Bixbyite	$(Mn,Fe)_2O_3$	3+	5.12	Paramagnetic
	Jacobsite	$MnFe_2O_4$	2+	4.99	Ferromagnetic
	Partridgeite	$a\text{-}Mn_2O_3$	3+	4.95	
Carbonate ore	Kutnohorite	$CaMn(CO_3)_2$	2+	3.11	
	Rhodochrosite	$MnCO_3$	2+	3.69	Paramagnetic
Other	Galaxite	$MnAl_2O_4$	2+	4.03	

References: *www.mindat.com; Post, 1999; Cairncross and Beukes, 2013; Elliot and Barati, 2020; Beukes et al., 2016; Singh et al., 2020.*

*Density and magnetism are important mineral properties that may exploited in respectively gravimetric and magnetic exploration surveys for Mn mineralisation, particularly within silicate lithologies (which are typically less magnetic and less dense; e.g., Murthy et al., 2009). Other mineral properties that may be exploited during Mn exploration include its electrical properties (e.g., resisitivity and chargeability), with several case studies highlighting the applicabity of combining geoelectrical techniques (e.g., induced polarisation, resisitivity, and self-potential surveys; Ramazi and Mostafaie, 2013; Srigutomo et al., 2016).

2013). Todorokite is one of the major components of deep-sea Mn nodules and, because of the large size of tunnels, probably it is the host for nickel, cobalt and copper. Lithiophorite ($(Al,Li)Mn^{4+}O_2(OH)_2$), birnessite ($Na^{4+}Mn_{14}O_{27}{\cdot}9H_2O$), and vernadite ($\delta\text{-}MnO_2$) are the most common tetravalent Mn oxides with sheet structures. Lithiophorite is a common supergene mineral and is also present in low temperature hydrothermal deposits. It is composed of alternating sheets of MnO, and (Al,Li)(OH) octahedra.

More crystalline Mn^{4+} minerals are associated with vein-fill material and include pyrolusite (MnO_2), cryptomelane (KMn_8O_{16}) and romanèchite ($(Ba,H_2O)_2Mn_5O_{10}$), finely intergrown assemblages of which are collectively referred to as 'manganomelane minerals' in this text. Pyrolusite is a tetragonal Mn oxide composed of a framework of square tunnels formed by single edge-sharing MnO octahedra, whereas cryptomelane and romanechite are monoclinic Mn oxides. Divalent and trivalent Mn-oxides are more strongly associated with diagenetic assemblages and hypogene hydrothermal processes which have upgraded pre-existing Mn-bearing protolith. These include the silica-containing oxide minerals braunite I (Mn_7SiO_{12}) and braunite II ($Ca(Mn,Fe)_{14}SiO_{24}$), which crystalise in the tetragonal system as pyramidal striated crystals or as masses, and the Mn oxide phases hausmannite (Mn_3O_4) and partridgeite ($\alpha\text{-}(Mn_2O_3)$) which are tetragonal and orthorhombic respectively. Mixed Mn and Fe oxides include jacobsite ($Mn^{2+}Fe^{3+}O_4$) and bixbyite ($(Mn^{3+},Fe^{3+})_2O_3$). Rhodochrosite ($MnCO_3$) and kutnohorite ($CaMn(CO_3)_2$) are the two common Mn-bearing trigonal carbonate minerals. Although kutnohorite is the more prevalent ore mineral in the KMF, rhodochrosite is a sought-after Mn carbonate because of its exquisite gem properties.

Ore forming processes pertinent to South African manganese deposits and occurrences

Numerous classification schemes have been proposed for Mn deposits and occurrences (Roy, 1988, 1997; Laznicka, 1992;

among others). Though we do not explicitly classify the South African occurrences into predefined deposit classes, we do provide a high-level overview of the general geological processes that serve to result in notable Mn enrichments in the Earth's crust. These processes broadly correlate to the genetic categories of Roy (1988, 1997) viz., sedimentary, hydrothermal and residual classes of Mn deposits. Further details of how these processes have manifested in the natural system are documented later in the text where the nuances of each RSA Mn deposit are discussed in a context of a temporal framework.

Incorporation of aqueous Mn^{2+} into carbonate minerals

A major repository of excess Mn in the Archaean and early-Proterozoic Earth system was the ambient surface waters, notably sea water, which is estimated to have had at least an order of magnitude more Mn than the modern ocean (Veizer et al., 1989). The primary reason for these enhanced Mn concentration levels is because Mn^{2+} is the dominant valence state under reducing conditions and this is much more soluble than the higher oxidation states (Mn^{3+}, Mn^{4+}) which predominate under modern-day oxidising surface conditions. The high Mn concentrations were thus available for incorporation into carbonate minerals during development of extensive Archaean carbonate platforms (e.g., Campbellrand and Malmani Subgroup carbonates of the Transvaal Supergroup). This incorporation takes place by co-precipitation and adsorption processes (e.g., Smrzka et al., 2019 and references therein) in which Mn^{2+} replaces the main divalent cations (e.g., Ca^{2+} (calcite), Mg^{2+} (dolomite), Fe^{2+} (siderite)) by cation substitution mechanisms. The elevated Mn concentrations in Archaean carbonate platforms may be an important consideration in forming residual Mn enrichments by later epigenetic processes.

Oxidation of aqueous Mn^{2+} in marine and lacustrine environments

Chemical sedimentation to form the precursors of bedded manganese (Mn) deposits

The most efficient way to deposit Mn out of solution in a chemical sedimentary environment is by oxidation of Mn^{2+} to Mn^{3+} and/or Mn^{4+}. This oxidation can occur via various possible oxidising agents or pathways (Robbins et al., 2023): oxygen (O_2); superoxide (O_2^-); nitrate (NO_3^-); sulphur (S^0); ferric iron (Fe^{3+}); anoxygenic photo-autotrophy; and photo-oxidation. This oxidation is typically either induced or mediated by biological activity, both in the presence of free O_2 (e.g., Tebo et al., 2004) and anaerobically through photochemical oxidation (e.g., Daye et al., 2019). The oxidation of Mn by free O_2 would require a source of oxygen, with oxygenic photosynthesis generally considered the only process to form significant quantities of free O_2 in surface environments (e.g., Holland, 2002; Godfrey and Falkowski, 2009). The abiotic oxidation of Mn by free O_2 has been found to proceed orders of magnitude slower than the biotic pathway (Diem and Stumm, 1984; Tebo, 1991; Stumm and Morgan, 1995; Tebo et al., 2004; 2005; Morgan, 2005; Konhauser, 2007; Namgung et al., 2018). The biotic pathway occurs via chemolithoautotrophy that oxidises Mn in the presence of free O_2 concentrations higher than approximately 7 µM (Tebo et al., 1984; Konhauser, 2007). The oxidation of Mn by anoxygenic photo-autotrophy, a biological process, has been proposed to explain some sedimentary Mn enrichments that pre-date the GOE (e.g., Johnson et al., 2013). However, although this process is well-known for Fe oxidation and bacteria have been identified (Konhauser et al., 2002; Smith, 2015), no bacterium has yet been identified in extant lineages for anoxygenic Mn photoautotrophs (Robbins et al., 2023). The only experiment that managed to biologically oxidise Mn in an anoxic medium could not isolate the responsible bacterium and was conducted in a sulphidic medium (Daye et al., 2019), indicating that it could have proceeded via the oxidised S pathway (Robbins et al., 2023). Superoxide is a product of NO_3^- photolysis (Jung et al., 2017), and NO_3^- also requires the presence of free O_2 to form (Godfrey and Falkowski, 2009; Thomazo and Papineau, 2013; Smith et al., 2017). However, in modern systems such as the Black Sea, oxidation of Mn by NO_3^- is ineffective (Schippers et al., 2005). Oxidation of Mn by oxidised S requires the production of the latter by anoxygenic photosynthesis (Van Cappellen et al., 1998; Katsev et al., 2004; Henkel et al., 2019; Robbins et al., 2023). Although the oxidation of Mn by Fe^{3+} could be possible under certain conditions, the reverse reaction, which is the reduction of Mn^{3+}/Mn^{4+} by Fe^{2+}, is favoured thermodynamically and was likely quantitatively more significant (Robbins et al., 2023). The final possible Mn oxidation mechanism, photooxidation, has been shown in experiments to convert rhodochrosite to Mn^{3+} oxyhydroxides (Liu et al., 2020). However, this has been questioned as a plausible mechanism because rhodochrosite was unlikely to have accumulated in the photic zone of early Earth's oceans (Lyons et al., 2020).

Experimental work (Murray et al., 1985) has shown that under controlled laboratory conditions, abiotic Mn^{2+} oxidation by O_2 is expected to lead to mixtures of mainly trivalent hydroxides of Mn (e.g., MnOOH polymorphs such as manganite) and/or mixed-valence minerals such as hausmannite (Murray et al., 1985; Namgung et al., 2018). Once formed, the poorly crystalline Mn oxide/oxyhydroxide colloids, and possibly Mn carbonate colloids (Wittkop et al., 2020), will have settled through the water column for preservation at the sea floor. The efficacy of this preservation may have been compromised by processes such as reduction of higher valence Mn colloids by reductants (e.g., organic matter, or Fe^{2+} at the iron redoxcline (e.g., Smith and Beukes, 2023; Smith et al., 2023)), or by remineralisation induced by biological activity.

Field evidence and known similarities in Fe and Mn chemistry (i.e., they are adjacent 3d transition metals on the periodic table) and redox chemistry, confirm that these two elements are intimately associated with one another in the natural environment. For example, both are soluble in their reduced states (Fe^{2+} and Mn^{2+}, respectively) at close to neutral pH (Figure 5a; Brookins, 1988). Thus, as the surface earth system became increasingly oxidising around the time of the Great Oxidation Event (GOE; Bekker et al., 2004; Gumsley et al., 2017; Poulton et al., 2021; Hodgskiss and Sperling, 2022), both elements were susceptible to rapid oxidation and precipitation.

Iron will oxidise more readily (i.e., at lower Eh or oxidising conditions) than Mn, whereas Mn will reduce more readily than Fe (Figure 5a; Brookins, 1988). The redox relationship between Fe and Mn has important implications for the deposition of these elements in chemical sedimentary environments and has led to certain vertical- and lateral depositional trends in the geological record. The Fe-Mn decoupling scenarios discussed here (Figures 5b to d) assume two conditions: a marine water body enriched in dissolved Fe^{2+} and Mn^{2+}; and oxidation as the main precipitation mechanism for Fe and Mn. These scenarios could also have been in effect together or separately depending on the depositional setting and could have been applicable to various water bodies enriched in dissolved Fe^{2+} and Mn^{2+}. These include low to increasing oxygen marine paleoenvironments of

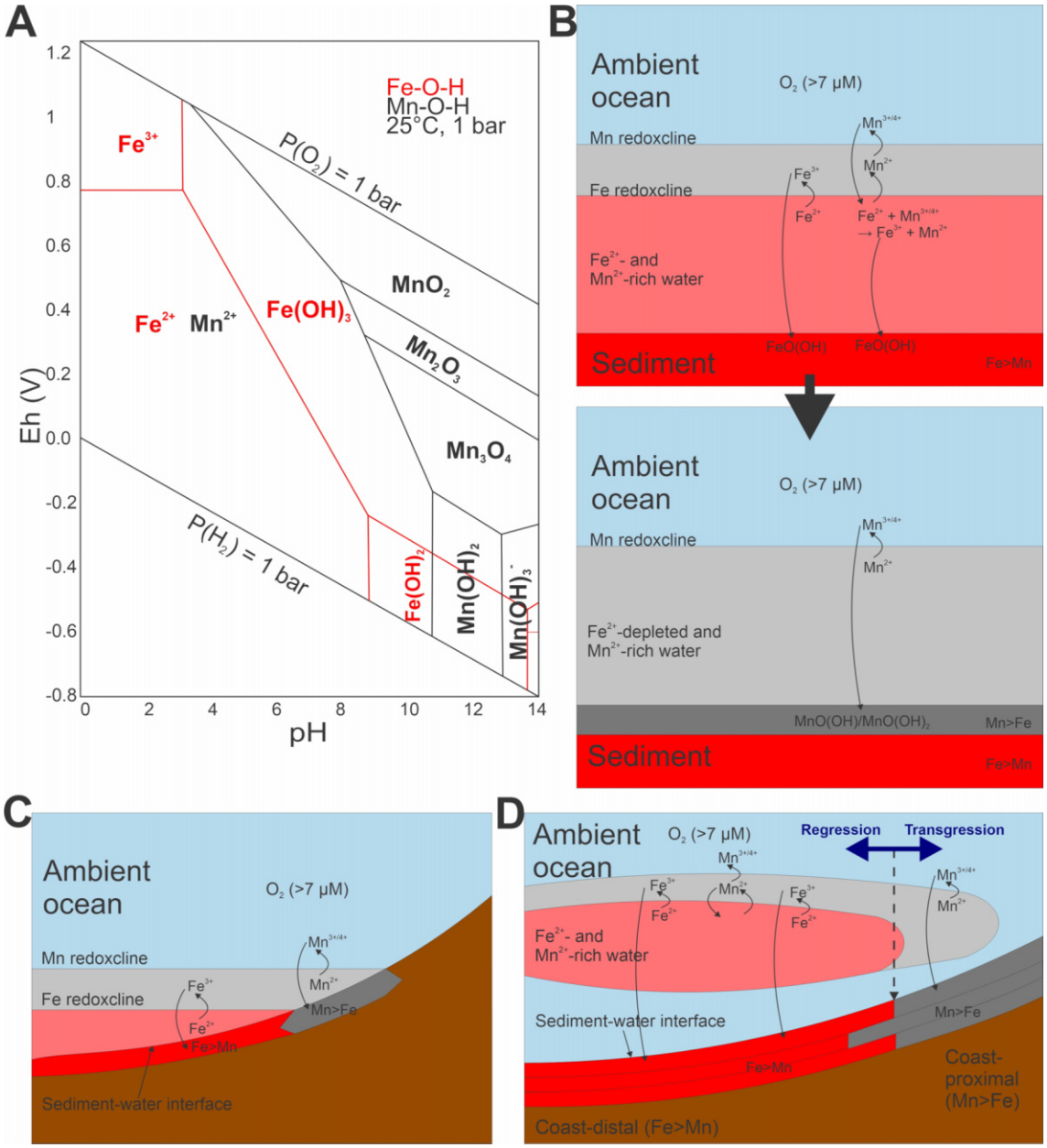

Figure 5. *(**A**) A combined iron (Fe) and manganese (Mn) Eh-pH diagram for the Fe/Mn-O-H system in an aqueous medium at a temperature of 25°C and a pressure of 1 bar (adapted from Brookins, 1988). (**B**) A diagram illustrating a simplified vertical depositional model for Fe and Mn from a Fe^{2+}- and Mn^{2+}-rich water column becoming progressively depleted in Fe^{2+} (adapted from Mhlanga et al., 2023). (**C**) A diagram illustrating a simplified lateral depositional model for Fe and Mn in a stagnant Fe^{2+}- and Mn^{2+}-rich water column as the Fe and Mn redoxclines reach the sediment-water interface towards the basin edge (adapted from Bühn et al., 1992; Beukes et al., 2016). (**D**) A diagram illustrating a simplified transgressive-regressive dynamic depositional model for Fe and Mn from a laterally moving Fe^{2+}- and Mn^{2+}-rich plume (adapted from Beukes et al., 2016; Smith and Beukes, 2023).*

the pre- to syn-GOE Earth (e.g., Kasting, 1992; Kendall et al., 2010; Planavsky et al., 2010; Czaja et al., 2012; Olson et al., 2013; Beukes et al., 2016; Mhlanga et al., 2023; Smith and Beukes, 2023); restricted or stagnant basins (e.g., Tebo et al., 1984; Tebo, 1991; Schippers et al., 2005); and basins with complete glacial ice cover during a Snowball Earth event (e.g., Klein and Beukes, 1993; Lechte and Wallace, 2016).

The first depositional scenario considers vertical sedimentary trends by assessing a fixed position in the basin (Figure 5b). It is likely that both an Fe and a Mn redoxcline, which is a horizontal zone where these elements are oxidised, would be established at different depths. Manganese oxidation would only become favourable once Fe^{2+} is depleted or no longer present due to the latter being a stronger reducing agent, indicating that the Mn redoxcline would occur above the Fe redoxcline (Figure 5b). A similar vertical trend has been observed in modern restricted basins such as the Black Sea (e.g., Lewis and Landing, 1991). Furthermore, any Mn^{3+}/Mn^{4+}-phases produced at the Mn redoxcline would settle through the water column until they encounter the Fe redoxcline, at which point they would be reduced back into solution by Fe^{2+}. As long as Fe^{2+} is still present in the water body, Fe deposition would be favoured and Mn deposition would be chemically inhibited. However, once most of the Fe^{2+} has been removed from the water column, the Mn^{3+}/Mn^{4+}-phases would form by oxidation and sediment out of the water column. This would then be preserved as Fe-rich sediment capped by Mn-rich sediment, as observed in sedimentary cycles of the Paleoproterozoic Hotazel Formation (Mhlanga et al., 2023) and the Neoproterozoic Otjosondu Mn and Fe deposits in Namibia (Beukes et al., 2016).

The second depositional scenario utilises the same redox relationship between Mn and Fe as described in the previous paragraph but considers lateral depositional trends. In this scenario a stagnant Fe^{2+}-rich and Mn^{2+}-rich water body is assessed at the sediment-water interface towards the edge of the basin (Figure 5c). This would be a similar scenario to the coastal margins of the Black Sea (Force and Maynard, 1991). As the basin shallows towards its edge, the Fe redoxcline will meet the sediment-water interface at some point. Iron deposition will be favoured from here towards the deeper water (i.e., in a coast-distal direction). The Mn redoxcline will reach the sediment-water interface closer to the coastline in shallower water than the Fe redoxcline. This would then be preserved as a sedimentary trend of Fe-rich sediment transitioning into Mn-rich sediment towards the palaeo-coastline, as observed in the Mesoarchean Vlakhoek Member of the Mozaan Group in southern Africa (Smith and Beukes, 2023) and the Otjosondu Mn and Mn deposits in Namibia (Bühn et al., 1992). This scenario is different from the one described previously (Figure 5b) in that complete Fe depletion from the water column is not required for Mn preservation in the sediment. The interplay between the Fe and Mn redoxclines and their loci relative to coastline geomorphology may be a dynamic process (Figure 5d), and resultant lateral depositional trends may be influenced by transgressive-regressive systematics which in turn are affected by external factors such as climate, tectonics, and orbital cycles. Such temporal variability may explain observations such as the repeat vertical transitional cycles of Fe to Mn and back into Fe again, as seen in the Hotazel Formation (Cairncross and Beukes, 2013; Beukes et al., 2016).

Fluid mixing and the development of oolitic manganese ores

The Tolwe Mn deposit, a South African deposit described in detail below, is a pisolitic Mn deposit suggested to have formed from the mixing of terrestrial Mn-bearing waters with alkaline marine waters in the presence of microbial mediation (Schaefer et al., 2001; Gutzmer et al., 2002). Briefly, the model invokes preferential leaching of Mn (relative to Fe) by slightly reducing groundwaters and/or fluvial waters and subsequent mobilisation to deltaic environments which mark maximum flooding surfaces during marine transgression. These shallow flooded delta plains represent the mixing interface between the terrestrial waters and marine waters, where the mixing interaction results in changes to the fluid physicochemistry, which in turn impact Mn solubility (Schaefer et al., 2001; Gutzmer et al., 2002).

Mechanisms for manganese precipitation in modern marine environments

Inasmuch as the processes described above are still active in the present day (e.g., chemical sedimentation of Mn in sub-oxic zones of the Black Sea (Lewis and Landing, 1991); Mn-enriched authigenic oolites in Lake Malawi (Williams and Owen, 1990)), perhaps the most important mechanism for Mn enrichment in the modern era is the formation of Mn-enriched nodules and crusts (e.g., Hein et al., 2013, 2020; Verlaan and Cronan, 2022). The importance of this process is highlighted by resource estimates made by Hein et al. (2013) who calculated that the contained Mn in just two of the crust- and nodule-enriched zones of the world's ocean was ~1.5 times the amount of Mn in the world's terrestrial reserve base. The ferromanganese nodules can grow to as large as 10 cm diameter and are typically found at depths between 3 500 to 6 500 m (Hein et al., 2020), whereas the thickest and most metal-rich crusts have been identified at depths of 800 to 2 500 m (Hein et al., 2013).

The nodules and encrustations form by hydrogenous processes, diagenetic processes, hydrothermal processes, or by a combination of these processes (Figure 6). The hydrogenous process involves direct precipitation of metals from the water column on to a mineral- or microfossil nucleus (for new nodules) or onto the surface of an existing Mn nodule. This process is relatively slow (growth rates of 2 to 5 mm per million years) and typically results in nodules that are particularly enriched in Co, Te, Ce and Pt (Verlaan and Cronan, 2022; Hein et al., 2020 and references therein). These elements are oxidised at reactive surface sites on the nodule surface, along with Mn and Fe which precipitate via autocatalytic oxidation processes (Crerar and Barnes, 1974). This sub-class of Mn nodule is used extensively to interpret changes in the flow regime and physicochemical characteristics of deep-water currents (i.e., Antarctic Bottom Water (e.g., Kasten et al., 1998; Ovechkina et al., 2021)). Nodule growth by diagenetic processes and by hydrothermal processes (in close proximity

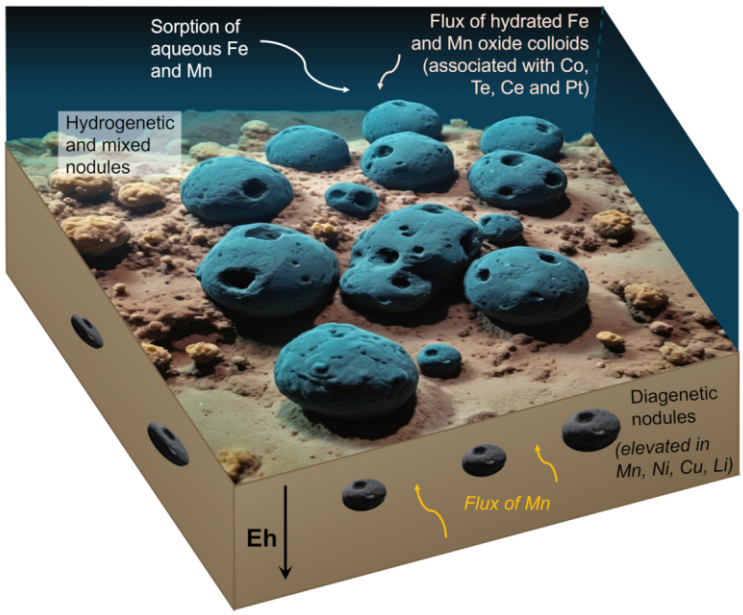

Figure 6. *Schematic illustrating the flux of iron (Fe) and manganese (Mn) from the water column to form hydrogenetic ferromanganese nodules, which may grow to up to 10 cm in diameter. Also shown is the flux of metals from porewaters (released as the Eh of the sediment decreases), which gives rise to diagenetic ferromanganese nodules. Part of this figure was created using generative artificial intelligence (AI).*

to a plume emanating from hydrothermal vent sites) are comparatively faster. The diagenetic nodules typically grow at rates up to 10 mm per million years, and precipitate at or below the sediment-water interface where upward migration of a more reduced and metal-laden pore water flux intersects an oxidation front close to or at the seabed. The diagenetic nodules are typically more enriched in Ni, Cu and Li where these elements serve to balance charge within the growing nodule's bulk chemistry (Hein et al., 2020, and references therein). Many nodules may be regarded as mixed in that they show mineralogical and chemical signals derived from both hydrogenetic and diagenetic processes. A growing body of work also highlights the likely role of biology in controlling the formation of ferromanganese nodules (Jiang et al., 2020, and references therein).

Diagenetic alteration of primary chemical precipitates

The chemical precipitates formed in the water column that do not undergo redox recycling ultimately sequester at the sea floor where they are later buried and subjected to diagenetic alteration. Diagenetic modification includes partial to complete mineralogical reconstitution of the primary precipitates, which were likely poorly crystalline Mn^{3+}/Mn^{4+} oxyhydroxides (Calvert and Pedersen, 1996; Yan et al., 2022; Mhlanga et al., 2023; Smith et al., 2023) and possibly Mn^{2+} carbonates (Wittkop et al., 2020) and silicates (Coetzee et al., 2024). A major process that acted on these primary precipitates below the sediment water interface was likely a bacterially mediated reduction process coupled with organic matter oxidation (Myers and Nealson, 1988). This reduction process is similar to that of Fe^{3+} to Fe^{2+} via a process called dissimilatory iron reduction (DIR; e.g., Lovley, 1991). Primary Mn^{4+} species such as MnO_2 are implicated in diagenetic dissimilatory Mn reduction (DMR) through reactions such as follows:

$$CH_2O + 2MnO_2 + H_2O = 2Mn^{2+} + HCO_3^- + 3OH^- \quad (1)$$

The only key difference between Fe and Mn in this context is that for every mole organic C oxidised, only two moles of tetravalent Mn species will be reduced. The dissolved Mn^{2+} produced by the above reaction can either be concentrated in the pore spaces or released back into the water column (Lovley, 1991). The Mn^{2+} remaining in pore space is readily available to form reduced Mn species, i.e., Mn carbonates such as rhodochrosite ($MnCO_3$), kutnahorite ($CaMn(CO_3)_2$), Mn-rich calcite, etc.

The strongly ^{13}C-depleted signal ($\delta^{13}C_{PDB}$ of ~-7 to -21‰ (Preston, 2001; Johnson et al., 2013; Mhlanga et al., 2023; Smith and Beukes, 2023; Smith et al., 2023)) in the Mn carbonates resulting from this DMR reaction suggests a significant involvement of a proportion of reactive organic carbon ($\delta^{13}C_{PDB}$ of -30 to -20‰; Freeman, 2001) along with dissolved inorganic carbon present in the marine realm ($\delta^{13}C_{PDB}$ of ~0‰; Faure, 1986). The mooted involvement of organic C corroborates the importance of biological processes in the formation of bedded Mn deposits, both at the oxidation stage in the water column (with organic detritus envisaged to sink along with settling Mn primary precipitates) and during bacterially mediated DMR.

Depending on local conditions, other Mn^{2+} and mixed-valence Mn species may also form as a product of diagenesis and subsequent metamorphism. These minerals include the oxides hausmannite, braunite and jacobsite, and the silicate friedelite, among others (Gutzmer and Beukes, 1996b and

references therein). The identification of Mn^{3+} as key redox player in sediment pore waters of modern hemipelagic sediments and in the water column of stratified euxinic basins such as the Black Sea (Trouwborst et al., 2006; Madison et al., 2013), raises the possibility that Mn^{3+} minerals may have played an important role as precursor candidates in ancient stratified basins. The prevalence of Mn^{3+} over Mn^{4+} also ties in well with the common occurrence of Mn^{3+}-rich diagenetic minerals, such as braunite which typifies diagenetic to low metamorphic assemblages of many ancient Mn deposits such as those of the KMF (Mhlanga et al., 2023). Manganese does not readily form diagenetic sulphide minerals unless the conditions of formation are sufficiently reducing and sulphidic to favour saturation in MnS (alabandite). There is thus a general paucity of such mineral species in the geological record (Hem, 1972).

Weathering and pedogenic processes

Residual accumulations of Mn form during deep weathering of precursor rocks that contain appreciable Mn, typically under hot and humid climatic environments. Carbonate precursor rocks are ideal for forming these Mn enrichments because they readily dissolve under acidic conditions, and because Mn^{2+} substitutes easily into the divalent metal coordination site in common carbonate minerals such as dolomite, calcite or siderite, leading to higher Mn concentrations in the precursor carbonates. On a macroscale, karstification of carbonate rocks is likely also important because the resultant topographic lows (represented by dolines and sink holes) serve as sites for accumulation and preservation of the Mn oxide wad. In the South African context, residual accumulations have developed above the Zandkopsdrif carbonatite complex (Harper et al., 2015) and in sideritic 'blackband' units of the Karoo Supergroup (van Niekerk et al., 1999; Pack et al., 2000). The chemical processes that give rise to these enrichments involve dissolution of the carbonate minerals by infiltrating acid and oxidising meteoric fluids, followed by preferential mobilisation of the carbonate and the major cations Ca and Mg. The acidity may be provided by carbonic acid formed by the reaction between water and CO_2 (Equation 2), with possible involvement by organic acids; and this acidity is consumed through the reaction with the carbonates (Equation 3).

$$CO_2 + H_2O \leftrightarrow H^+_{(aq)} + HCO_3^-{}_{(aq)} \quad (2)$$

$$Ca_{(1-x)}Mn_xCO_3 + 2H^+_{(aq)} \leftrightarrow CO_2 + (1-x)Ca^{2+}_{(aq)} + xMn^{2+}_{(aq)} + H_2O \quad (3)$$

At circumneutral pH, the dissolved Mn^{2+} may be oxidised (sluggishly) by abiotic processes to precipitate small and poorly-crystalline birnessite group minerals, or the kinetics of the oxidation reaction may be enhanced by microbial controls generally giving rise to very poorly crystalline δ-MnO_2 (Webb et al., 2005; Mayanna et al., 2015). Using a Mn enriched oxisol on the humid eastern escarpment of South Africa as a natural laboratory, Dowding and Fey (2007) provide a more involved process for Mn enrichment in soil profiles derived from underlying Mn-bearing carbonates (Figure 7). In this Al-enriched environment, the basal Mn enrichment located immediately above the regolith comprises lithiophorite as the dominant stable Mn phase. In the acidic, organic-rich top-soils, reductive dissolution results in the Mn repartitioning into nodules that comprise poorly crystalline Mn phases (Figure 7).

An alternative mechanism for Mn accumulation in soil environments is the formation of manganocretes under more arid conditions. This is caused by supersaturation of carbonate

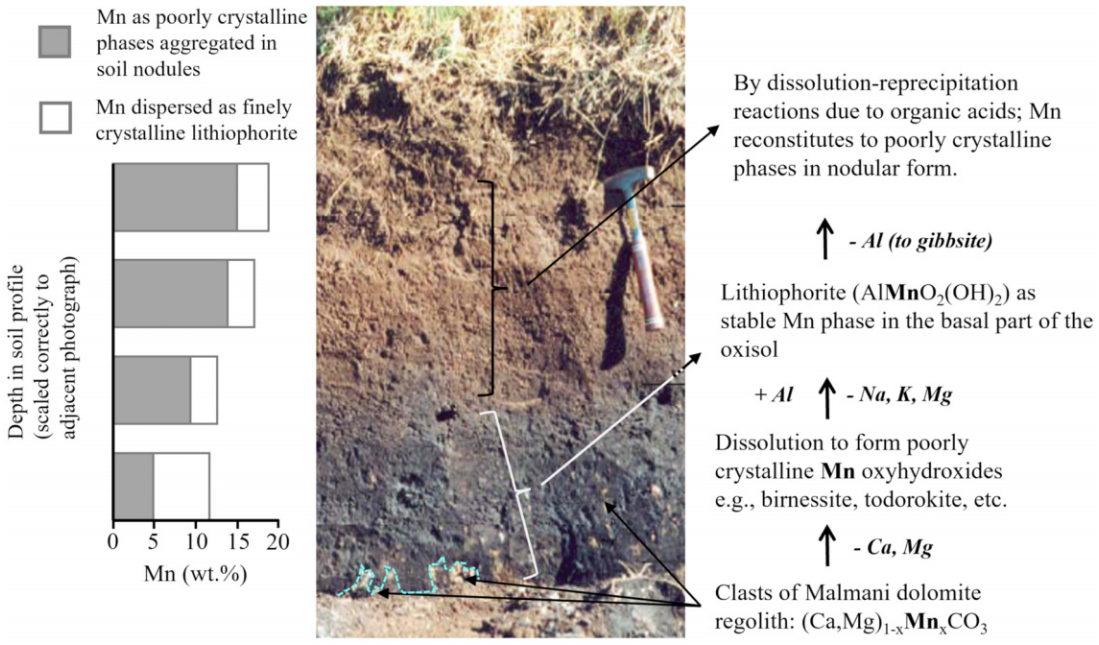

Figure 7. *Formation of residual manganese (Mn) enrichments in a modern oxisol soil profile in the Graskop area, which is located on the high rainfall and humid eastern escarpment (adapted from Dowding and Fey, 2007).*

ions and associated cations in the near-surface soil profile in response to water loss through evaporation and evapotranspiration (Equation 4). The excess carbonate thus bonds with available Mn to precipitate manganocrete or Mn enriched ferricretes. In the South African context, this is a relatively minor process with the only reported occurrences located above the Zandkopsdrif complex on the arid west coast (Harper et al., 2015).

$$2HCO_{3(aq)}^{-} + (1\text{-}x)Ca^{2+}_{(aq)} + xMn^{2+}_{(aq)} \leftrightarrow Ca_{(1-x)}Mn_xCO_3 + H_2O + CO_2 \quad (4)$$

Mobilisation and concentration by aqueous fluids

Manganese is highly mobile in some groundwater and in hydrothermal fluids where it complexes in its reduced divalent state predominantly as octahedral aqua- and chloro complexes (e.g., $[Mn(H_2O)_6]^{2+}$ and $MnCl^{+}_{(aq)}$; Gammons and Seward, 1996; Koplitz et al., 1994; Tian et al., 2014). In groundwater systems, Mn may be preferentially mobilised relative to geochemically-similar Fe if there is a slight drop in the Eh of the fluid (i.e., sufficient to reduce Mn but not Fe; Figure 5). Alternatively, if both Fe and Mn are mobilised, then fractionation may be achieved by increasing Eh to first oxidise Fe, leaving behind a residual Mn-enriched fluid for later precipitation at the ultimate trap site (e.g. Garcia et al., 2018). These trap sites are commonly structural in nature and form preferentially in rocks such as quartzites, which are more likely to behave in a brittle manner during low-temperature deformation than e.g., carbonates and shales. Examples of Mn deposits formed from fluids precipitating Mn in structurally-controlled trap sites include those in the Cape Supergroup, Waterberg Group, Pretoria Group (Timeball Hill and Polo Ground quartzites) and in the brecciated contact at the base of the Olifantshoek Group (Astrup and Tsikos, 1998). Although Mn solubility is enhanced as a function of increased temperature and salinity (e.g., Tian et al., 2014), Mn is also mobilised in groundwaters and in relatively low-temperature chalybeate (i.e., ferruginous and manganiferous) hot springs. Locally, Mn mounds may develop where manganiferous hot springs expel at surface (de Villiers, 1960; von der Heyden et al., 2024). Higher-temperature hydrothermal venting associated with exhalative base metal and barite deposits may also efficiently precipitate Mn at the mixing interface with cool ocean bottom waters, as has been suggested for localised Mn deposits in the Bushmanland Subprovince of the Namaqua Metamorphic Belt (Coetzee, 1958; Astrup and Tsikos, 1998).

A second manner in which warm hypogene fluids may be involved in the genesis of Mn deposits is when they traverse Mn-enriched protoliths. Here, rather than providing an addition of extraneous Mn to the rock mass, the fluids play a more important role in upgrading the Mn content of the rock by removing other non-economic cations and anions. A good example of this mechanism is evidenced by the Wessels alteration event during which carbonate minerals were preferentially leached from the Mamatwan-type proto-ores. This led to ore upgrade (35 to 38% Mn upgraded to 45 to 60% Mn), changes to the mineralogy (braunite-kutnohorite ores to hausmannite-rich oxide assemblages), mass loss, and a ~30% reduction of the thickness of the ore beds (Gutzmer and Beukes, 1997a).

A temporal overview of South Africa's Manganese deposits and occurrences

South Africa has a rich and well-preserved geological history that extends as far back as 3.6 billion years. Several works have documented temporal changes in Mn speciation and enrichment as a function of time (Hummer et al., 2022; Roy, 1997). Here we follow precedent and present the local Mn enrichments in accordance with their temporal genesis. Figure 1 and Table 3 summarise the results of this approach, highlighting that although multiple lithostratigraphic units host the RSA Mn deposits, their formation can generally be attributed to discrete geological events (e.g., the development of unconformity surfaces that cut multiple lithostratigraphic units). These events notably include the Great Oxidation Event (GOE), and the formation of the Pre-Gamagara unconformity and the African- and Post-African unconformity surfaces.

Manganese deposits formed prior to the Great Oxidation Event (i.e., > ~2.4 Ga)

The GOE marks the first significant increase in the Earth's atmospheric oxygenation (Holland, 2002; Luo et al., 2016) and occurred between approximately 2.47 and 2.19 Ga (Bekker et al., 2004; Luo et al., 2016; Gumsley et al., 2017; Poulton et al., 2021; Hodgskiss and Sperling, 2022). The main line of evidence for the GOE is the sudden disappearance of S mass independent fractionation (SMIF) from the geological record around this time, implying the first establishment of an ozone layer (e.g., Farquhar et al., 2000; Luo et al., 2016). Considering the importance of free O_2 for the sedimentary deposition of Mn, it is not surprising that the first and largest significant sedimentary Mn deposit occurs in the approximately 2.4 Ga Hotazel Formation (Beukes et al., 2016; Gumsley et al., 2017), with pre-GOE sedimentary Mn enrichment being rare. However, southern Africa's geological record contains some unique pre-GOE sedimentary Mn enrichments that, although not economic, are of broader paleoenvironmental significance.

Significant pre-GOE Mn enrichments (i.e., >7 and up to 47 wt.% MnO) occur within multiple units of the Mesoarchean Mozaan Group of the Pongola Supergroup (Planavsky et al., 2014; Ossa Ossa et al., 2016; Albut et al., 2018; 2019; Smith and Beukes, 2023) and West Rand Group of the Witwatersrand Supergroup (Smith et al., 2023). These successions also show a strong geochronological overlap (~2.96 to 2.91 Ga) and lithostratigraphic correlation (Beukes and Cairncross; 1991), with some of the Mn-rich beds also correlating with one other (Smith et al., 2023). This implies that they were deposited as part of the larger Witwatersrand-Mozaan basin during the Mesoarchean (Beukes and Cairncross; 1991; Smith, 2018). From the base upwards, Mn-enriched units in this succession includes the Vlakhoek Member Fe-formation of the Sinqeni Formation (Planavsky et al., 2014; Albut et al., 2018; Smith and Beukes,

Table 3. Summary of noteworthy South African manganese (Mn) deposits and occurrences (see main text for applicable references)

Deposit	Mineralisation control	Host rock	Age of Host	Age of mineralisation	Main ore minerals	Grade
Marine Mn nodules	Autocatalytic precipitation from water column, oxidation of pore water flux	Current sea floor	0 Ma	15 to present	Vernadites, todorokite, birnessite	8 to 22% Mn
Cape sinter deposits	Subaerial oxidation of chalybeate springs	Current land surface (typically linked to Cape Supergroup aquifer systems)	0 Ma	Ongoing	Poorly crystalline manganomelane minerals	up to 40% Mn
Eastern escarpment oxisols	Pedogenic processes; supergene residual accumulation	Current land surface above Malmani Dolomites	2.5 to 2.6 Ga	Ongoing	Lithiophorite, birnessite, todorokite, nsutite	up to 17% Mn
Cape structure-hosted occurrences	Oxidation of groundwater Mn flux	Cape Supergroup (predominantly quartzites)	~400 Ma	Unconstrained, likely recent. Structures possibly formed during development of Cape Fold Belt.	Cryptomelane, psilomelane, pyrolusite, nsutite	25 to 56% Mn
Waterberg stucture-hosted occurrences	Likely oxidation of groundwater Mn flux	Basal units of Waterberg Group	~2 Ga	Unconstained. Structures possibly related to movement along the long-lived Thabazimbi-Murchison lineament.	Likely manganomelane group minerals	24% Mn
Zandkopsdrif carbonatite	Supergene residual accumulation, locally manganocretisation	Carbonatite	55 Ma	Post-African 1 erosion surface (~15 Ma)	Pyrolusite, psilomelane (romanechite)	5.1% Mn
North West Mn Field	Supergene residual accumulations	Formed above Malamani dolomite (and also weathered Ecca Group rocks of the Karoo Supergroup)	Variable	Post-African 1 erosion surface (~15 Ma)	Varies between mines: romanechite, cryptomelane, galaxite, pyrolusite, amorphous Mn	up to 23% Mn
Namaqua exhalites	Hot hypogene fluid expelling in cooler subaqueous settings	Bushmanland Subprovince metasediments	~1.2 Ga	~1.2 Ga (syn-sedimentary)	Jacobsite, bixbyite, pyrolusite, cryptomelane and psilomelane	up to 26% Mn
Tolwe oolitic Mn	Fluid mixing in a deltaic environment	Soutpansberg Group	1.8 to 1.96	1.8 to 1.96 Ga (syn-sedimentary)	Braunite	30 to 41% Mn
Postmasburg Mn Field: eastern belt	Residual accumulations in karst environment	Campbellrand dolomite	2.5 to 2.6 Ga	Pre-Gamagara unconformity surface (~2.0 Ga)	Siliceous Mn ore: Braunite (minor partridgeite)	45 to 59% Mn
Postmasburg Mn Field: western belt	Debated: residual accumulation versus hypogene fluid flow, with later alterations	Campbellrand dolomite	2.5 to 2.6 Ga	Pre-Gamagara unconformity surface (~2.0 Ga)	Ferruginous Mn ore: Braunite, partridgeite	32 to 46% Mn
Rooinekke Mn deposit	Residual accumulation from weathering of Mn-rich carbonates	Koegas subgroup BIF	~2.4 Ga	Pre-Gamagara unconformity surface (~2.0 Ga)	Jacobsite, braunite, hausmannite	~35% Mn
Kalahari Mn Field: Mamatwan-type	Chemical sedimentation at or near Great Oxidation Event	Hotazel Formation BIF	~2.4 Ga	~2.4 Ga	Braunite, kutnohorite (plus local later supergene enrichment)	30 to 38%
Kalahari Mn Field: Wessels-type	Hypogene upgrade of Mamatwan-type proto-ores	Hotazel Formation BIF	~2.4 Ga	~1.2-1.0 Ga	Haussmanite, bixbyite, braunite II	46 to 55%
Pre-GOE Pongola Mn occurrences	Chemical sedimentation	Localised occurrences in Witwatersrand and Pongola Supergroups	~2.9 Ga	~2.9 Ga	Mn^{2+} carbonates	>5.4% to 36% Mn

*BIF=Banded Iron Formation; GOE=Great Oxidation Event

2023), the Mhlatuze Member Fe-formation and Fe-rich shales of the Ntombe Formation (Ossa Ossa et al., 2016), two Fe-rich shales within the Thalu Formation and an Fe-rich shale at the top of the Brixton Formation (Smith et al., 2023).

Within unaltered samples in these Mesoarchean units, all the Mn is present as Mn^{2+} hosted in Mn-rich carbonates. There has been no documentation of Mn^{3+} such as is preserved in braunite in the Paleoproterozoic Hotazel Formation (Gutzmer and Beukes, 1996b; Mhlanga et al., 2023). Despite the lack of any preserved oxidised Mn, there is strong evidence that Mn oxidation was the main precipitating mechanism in the ocean water column. For example, the Mn-rich carbonates show petrographic evidence for diagenetic formation and are highly depleted in ^{13}C ($\delta^{13}C_{PDB}$ of ~-22 to -7‰), implying formation through a redox reaction between Mn^{3+}/Mn^{4+} and organic carbon (Smith and Beukes, 2023; Smith et al., 2023). The Mn/Fe ratio shows a strong negative correlation with Mo isotope values ($\delta^{98}Mo$), implying that Mn oxidation and the subsequent formation of Mn oxides were responsible for Mo transfer into the sediment (Planavsky et al., 2014; Albut et al., 2018). In the Fe isotopic system, the $\delta^{56}Fe$ values show more depleted signatures with increasing Mn contents (Albut et al., 2019), implying that advanced Fe oxidation (i.e., decreasing isotope values; Planavsky et al., 2009) had to take place before Mn could be deposited (Smith and Beukes, 2023). This is corroborated by sedimentological evidence from the Witwatersrand-Mozaan basin, where Mn enrichment with concomitant Fe depletion can be tracked from deeper water into shallower water deposition in multiple units (Smith and Beukes, 2023; Smith et al., 2023). The implication is that Fe^{2+} had to have been depleted in the water column for Mn deposition to become significant, suggesting a redox buffering of Mn oxidation by Fe^{2+} (Figures 5b to d).

As previously discussed, Mn oxidation strongly implies the presence of free oxygen in the depositional environment. This has led to the proposal of a Mesoarchean "oxygen oasis" in the Witwatersrand-Mozaan basin that pre-dated the GOE by approximately 500 million years (Planavsky et al., 2014; Albut et al., 2018). This has also been supported by combined sulphur-iron isotopes in diagenetic pyrites from the Nsuze Group underlying the Mozaan Group (Eickmann et al., 2018).

Chemical sedimentation around the time of the Great Oxidation Event: The Kalahari Manganese Field (~2.41 Ga)

The KMF is the largest single deposit of Mn in the continental geological record. With an estimated 4200 Mt of Mn metal, it represents well over 70% of the world's total continental Mn resource (Beukes et al., 2016). The KMF comprises chemical sedimentary rocks of the Hotazel Formation, an interlayered sequence of banded Fe formation (BIF) and Mn-rich chemical sedimentary rock, also termed Mn formation (MnF) in three laterally continuous sedimentary cycles (Figure 8) (Kleyenstuber, 1984; Nel et al., 1986; Gutzmer and Beukes, 1995; Tsikos and Moore, 1997; Schneiderhahn et al., 2006; Tsikos et al., 2003, 2010; Mhlanga et al., 2023). The lowermost of these cycles hosts the thickest and economically most important Mn layer, which can attain a maximum stratigraphic thickness of ~45 m (Beukes et al., 2016). The Mn contents vary both vertically and laterally within each cycle and also vary across the three different cycles.

The Hotazel Formation forms the lower formation (overlain by the Mooidraai Formation carbonates; Figure 8) of the uppermost Voëlwater Subgroup of the Neoarchaean-Palaeoproterozoic Transvaal Supergroup in the Griqualand West Basin of the Northern Cape Province. The depositional age of the Hotazel Formation has been constrained to between approximately 2.38 Ga and 2.41 Ga (Bau et al., 1999; Gumsley et al., 2017; Schier et al., 2020). This places the Hotazel strata at a time in geological history that corresponds broadly to the period leading up to or overlapping with the GOE. Arguably the key feature of the Hotazel Formation is its conspicuous interlayering between Mn-rich sedimentary rock and BIF (Figure 8). This is a unique feature in the context of pre-GOE BIFs across the globe, which contrasts sharply with the paucity of Mn from practically every BIF that has been reported in the literature from the same period. The dearth of Mn in BIF has been previously attributed to the reductive capacity of Fe^{2+} in the Precambrian ferruginous oceans, which would have effectively recycled any transiently oxidised form of Mn back

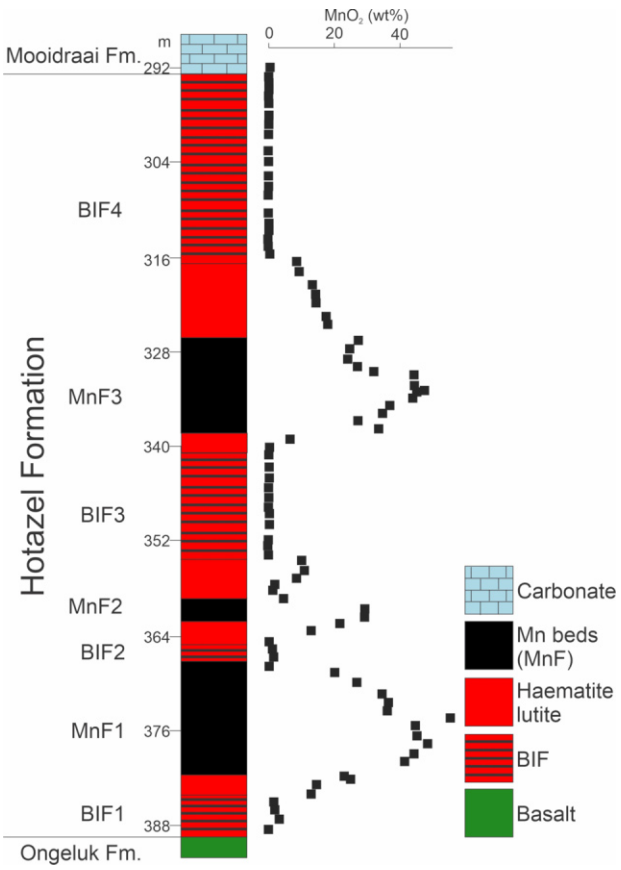

Figure 8. *The lithostratigraphy and vertical manganese (Mn) content variations of the ~2.41 Ga Hotazel Formation from a borehole drilled at the Gloria Mine in the northern Main Kalahari Deposit of the Kalahari Manganese Field (KMF) (adapted from Mhlanga et al., 2023).*

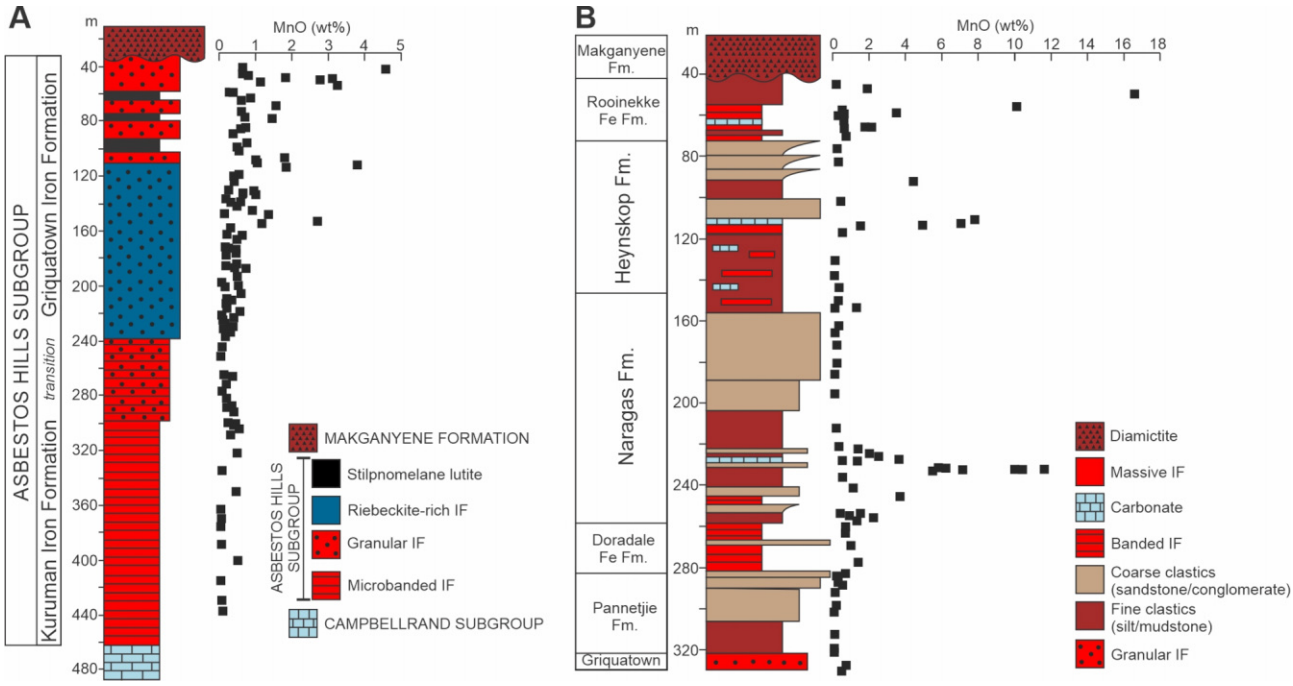

Figure 9. *Manganese (Mn) concentrations in the bulk rock from drill core of the ~2.44 Ga Asbestos Hills (**A**) (adapted from Oonk et al., 2017; Siahi et al., 2020) and ~2.42 Ga Koegas (**B**) (adapted from Schröder et al., 2011) subgroups in the Griqualand West Basin of the Transvaal Supergroup. Both subgroups show gradual increases in the MnO content in the lead-up to the Great Oxidation Event (GOE) and prior to the deposition of the Hotazel Formation, which hosts the Kalahari Manganese Field (KMF). Drill core locations are directly south of Hotazel for the Asbestos Hills Subgroup and directly west of Griquatown for the Koegas Subgroup.*

into seawater as soluble Mn^{2+} (Figure 5). Simple mass-balance considerations based on iron isotope systematics and Fe/Mn concentration ratios in BIF, provide support for a long-term Rayleigh fractionation effect (i.e., continual, preferential removal of Fe relative to Mn) in the Precambrian ocean (Tsikos et al., 2010). The model predicts that the protracted deposition of Mn-lean BIF would have led to progressive enrichment of Mn relative to Fe in the early ocean, and a concomitant depletion in isotopically heavy Fe that preferentially sequestered in earlier-precipitated BIF. Such a scenario points to a terminal Paleoproterozoic marine realm with sufficient aqueous Mn enrichment to produce a sedimentary sequence such as the Hotazel Formation (Tsikos et al., 2010). The Rayleigh model of Tsikos et al. (2010) finds additional support in the relatively high Mn contents recorded in the BIF sequences that stratigraphically precede the Hotazel Formation, namely the uppermost Griquatown Formation of the Asbestos Hills Subgroup (Oonk et al., 2017; Siahi et al., 2020) and the Koegas Subgroup (Schröder et al., 2011; Kurzweil et al., 2016). The uppermost part of the Asbestos Hills BIF displays gradually increasing Mn concentrations (Siahi et al., 2020; Figure 9a) which – albeit of no economic significance – appear to be the start of increasing Mn concentrations in the Transvaal Supergroup. Even higher Mn abundances are recorded in multiple formations of the overlying Koegas Subgroup (Figure 9b) (Schröder et al., 2011; Johnson et al., 2013), lending additional support to the significance of this apparent Mn build-up in global redox terms that precedes the Hotazel Formation.

Arguably the key difference between the Mn peak at the top of the Asbestos Hills Subgroup (Figure 9a), the Mn peaks within the Koegas Subgroup (Figure 9b) and the three striking Mn layers of the Hotazel Formation (Figure 8), is in the respective mineralogical modes of Mn. In the case of the uppermost Griquatown BIF, the Mn is exclusively hosted in a diluted fashion as Mn^{2+} in the carbonate fraction of the rocks and appears to be derived from primary precipitation of Mn-rich Mg calcite, remnants of which have been described by Siahi et al. (2020). In the Koegas Subgroup the Mn is also exclusively hosted as Mn^{2+}, but in a more concentrated fashion in kutnohorite. This was likely a product from the previously mentioned diagenetic redox reaction (reaction [1]) between oxidised Mn and organic carbon (Johnson et al., 2013; Beukes et al., 2016), indicating that Mn oxidation started to become more common, but did not exceed organic C in the ratio as set out in reaction [1]. By contrast, significant Mn in the Hotazel Formation is concentrated in the common ore mineral braunite as Mn^{3+}, indicating that oxidation of Mn^{2+} to at least its trivalent state and its preservation during diagenesis became a key process that distinguishes the depositional style of the Hotazel rocks from that of older BIF. Reduction of Mn^{3+} by organic C was still a key process (Mhlanga et al., 2023), but produced Mn^{3+} was now in excess of the ratio to organic carbon set out in reaction [1]. The strongly oxidising conditions required were also proposed by Schier et al. (2020) based upon the presence of true negative Ce anomalies in the Mn beds of the Hotazel Formation. Mhlanga et al. (2023) concluded that

the Hotazel Formation represents the first major chemical sedimentary record in Earth history that records significant oxidation of Mn^{2+} to Mn^{3+}, followed by large-scale deposition and preservation of the latter as three sedimentary cycles modulated by corresponding fluctuations in sea level.

Most previously published depositional models for the Hotazel Formation infer Fe^{2+}- and Mn^{2+}-enriched waters undergoing progressive oxidation from source to sink, with Mn deposition and preservation becoming dominant as Fe^{2+} becomes depleted (Figure 5d) (e.g., Cairncross and Beukes, 2013; Beukes et al., 2016; Mhlanga et al., 2023). There are only differences in the depositional settings proposed, ranging from a back-arc basin (Beukes et al., 2016) to a passive margin-style depositional setting (Mhlanga et al., 2023). It should be noted that alternative models on the formation of the Mn enrichment in the Hotazel Formation have been proposed. One alternative is that the Hotazel Formation is a volcanic exhalative deposit, similar to modern day mid-ocean ridge deposits (Cornell and Schutte, 1995). This model does not deviate from the redox processes that could have caused deposition of the Fe and Mn, but rather proposes an alternative source that provided the Fe and Mn to the seawater (exhalation instead of upwelling), and a different depositional setting. This exhalative model was supported in part by a slightly positive Eu anomaly in chondrite-normalised rare earth element (REE) data (Cornell and Schutte, 1995). However, support for this model diminishes if the more contemporary approach of shale-normalisation of REE data is used, since this indicates an absence of an Eu anomaly and temperatures below approximately 350°C (Schier et al., 2020). Another proposed alternative is that the Mn enrichments are post-depositional and that upwards migrating Mn-enriched hydrothermal or metasomatic fluids encountered microbial mats in sediment, leading to Mn-carbonate mineralisation (Kuleshov, 2012).

Supergene enrichment at the pre-Gamagara unconformity: development of the Postmasburg Manganese Field and manganese ore occurrences in the Koegas Subgroup (2.2 to 2.0 Ga)

The Postmasburg Manganese Field (PMF) contains deposits that evidently formed in an ancient, oxidising continental environment, either at the interface between land and atmosphere during weathering, or under localised subterranean (cave) and subaqueous (lacustrine) conditions (Beukes, 1983; Beukes et al, 2002, 2003; Gutzmer and Beukes, 1996a; 1997b). The PMF deposits are found in the geographic region south of the KMF, specifically in the eastern and western limbs of a major anticlinal structure known as the Maremane Dome (Figure 10) (see Figure 3 in Smith and Beukes, 2016 for cross-section). The Maremane Dome exposes carbonate rocks (chiefly dolostones) of the Campbellrand Subgroup, which dominate the lower stratigraphic portion of the Transvaal Supergroup (Figure 9). The Maremane Dome hosts world-class iron ores which are found in karstic depressions ("sinkholes") containing Mn-lean, massive haematite ore, thought to have formed at the expense of collapsed iron formations of the Asbestos Hills Subgroup that regionally overlies the Campbellrand dolostones (Gutzmer and Beukes, 1996a; Smith and Beukes, 2016). Manganese-rich deposits in the PMF are spatially associated with these iron ore deposits and occur in two modes:

- karstic "linings" of massive, siliceous Mn-rich material ("eastern belt" ores) in association with an interpreted

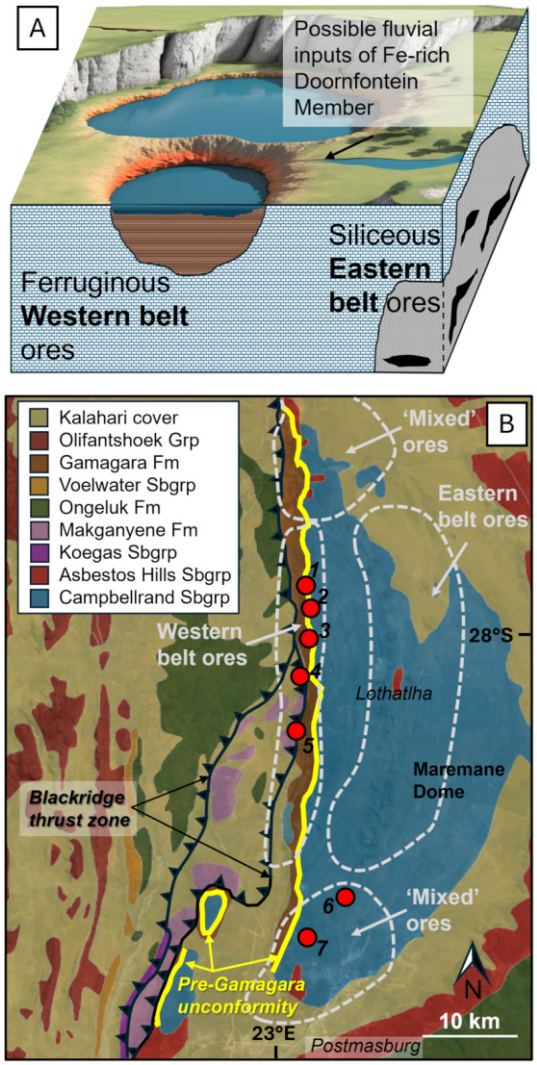

Figure 10. *(**A**) Generalised schematic showing the geological settings associated with the precursors to the two different ore types in the Postmasburg Manganese Field (PMF). The ferruginous western belt ore was associated Al-rich bauxitic material and manganese (Mn) wad, whereas the siliceous eastern belt ore was associated with chert 'Wolhaarkop' breccia in karstic cavities. Both ores experienced modification by metamorphic/ supergene/hypogene processes. Part of this figure was created using generative AI. (**B**) Regional geological map showing the location of the different ore types in the PMF (after Fairey et al., 2019) and their spatial relationship with the two key structures postulated to control the ore genesis viz. the pre-Gamagara unconformity surface and the Blackridge thrust. Numbers provide the active Mn mine locations (from the www.amaranthcx.co.za cadastre): 1=Boskop; 2=Bishop; 3=Morokwa; 4=Lohatlha; 5=Emang (Glosam); 6=Kareepan; 7=Pensfontein. Background map from Google Earth imagery, and geological overlay is from the Council for Geoscience 1:1000 000 geological map.*

solution collapse breccia developed atop weathered dolostone; and
- laminated, ferruginous deposits ("western belt" ores) associated with Gamagara-Mapedi shales of the Keis Supergroup (von Plehwe-Leisen and Klemm, 1995; Gutzmer and Beukes, 1996b; 1997b; Figure 10).

A few schools of thought prevail with regards to the genesis of these irregular Fe/Mn ore deposits of the PMF (see Figures 5 and 8 in von Plehwe-Leisen and Klemm, 1995; Figures 3 and 4 in Gutzmer and Beukes, 1997b; Figure 12 in Fairey et al., 2019). The first invokes a hydrothermal origin for the Fe and Mn mineralisation due to the seemingly very complex and diverse range of mineral phases present. De Villiers (1944) suggested that the mineralisation of Fe and Mn was due to structurally controlled circulating meteoric fluids that were heated at depth by magmatic vapour. These hydrothermal fluids would have leached the underlying Campbellrand dolomites of both Fe and Mn and transported both metals in solution. Precipitation of Fe and Mn oxides would have occurred once the metalliferous solutions encountered oxidised meteoric waters at shallower depth. The second and arguably the more widely-accepted genetic model for Mn (and Fe) mineralisation in the PMF, involves karstification of Mn-rich dolomite of the Campbellrand Subgroup during a period of erosion prior to the deposition of shales of the Gamagara/Mapedi Formation (von Plehwe-Leisen and Klemm, 1995; Gutzmer and Beukes, 1996a, 1997b) along the pre-Gamagara/Mapedi unconformity (Smith and Beukes, 2016). This is essentially a paleo-supergene model of ore formation which subdivides the deposits into two classes, namely eastern and western belt ores, based on their characteristic Fe/Si ratios. Another possible genetic fingerprint of the PMF ores implicates alkali metasomatism, which produced gangue assemblages of silicate species such as K-feldspar and albite and a suite of rare silicate minerals such as sugilite, norrishite and armbrusterite (Moore et al., 2011). This hydrothermal event is thought to have affected the Transvaal Supergroup rocks on a regional scale, from the PMF to the KMF in the late Neoproterozoic (Moore et al., 2011; Fairey et al., 2019).

Mineralogically, the Mn ores of the PMF are also very complex, with the main mineral species observed representing different paragenetic stages of ore formation such as primary deposition, diagenesis, metamorphism, hydrothermal alteration, and supergene alteration. The detrital to diagenetic component of these ores has been reported to include minerals such as quartz (von Plehwe-Leisen and Klemm, 1995; Gutzmer and Beukes, 1996b), whilst minerals such as hematite, braunite, partridgeite, bixbyite and hausmannite mostly formed during the diagenetic and metamorphic stages of ore formation (von Plehwe-Leisen and Klemm, 1995; Gutzmer and Beukes, 1996b; Fairey et al., 2019). A supergene and/or hydrothermal stage produced other phases such as pyrolusite, cryptomelane, Mn wad etc. (Gutzmer and Beukes, 1996b), whilst the alkali-rich assemblages mentioned above are thought to represent metasomatic alteration (Moore et al., 2011).

Another Mn ore enrichment related to supergene weathering along the pre-Gamagara/Mapedi unconformity occurred in the Rooinekke Formation of the Koegas Subgroup (Beukes et al., 2016). The previously mentioned Mn-enriched carbonate-bearing lithologies were oxidised when exposed by the pre-Gamagara/Mapedi unconformity surface to develop ancient wad-type Mn accumulations. Subsequent diagenesis and regional metamorphism altered these wad accumulations into braunite-hausmanite-jacobsite ore deposits exploited historically by underground mining at the Rooinekke Manganese Mine (Beukes et al., 2016). This event also formed supergene high grade iron ore deposits in the Rooinekke Formation (Smith and Beukes, 2016).

The world's earliest oolitic-pisolitic manganese ores: Tolwe (1.8 to 1.9 Ga)

The *ca.* 1.8 to 1.96 Ga Tolwe (or Bronkhorstfontein) Mn deposit is regarded as the oldest known example of oolitic-pisolitic Mn mineralisation globally (Schaefer et al., 2001; Gutzmer et al., 2002; Beukes et al., 2016). Despite this acclaim, the occurrence has received surprisingly little scientific attention since the publications in the early 2000s, the findings of which are briefly summarised here. The occurrence has also not received recent economic attention, despite an estimated remaining resource of 10 to 15 Mt braunite ore grading at 30 to 41% Mn (Astrup and Tsikos, 1998; Gutzmer et al., 2002). The Tolwe occurrence comprises five manganiferous seams that formed towards the top of the Wyllies Poort Formation, specifically in the Roodeberg erosional outlier which lies to the west of the main Soutpansberg basin. Each of these Mn seams lies at the top of an upward coarsening sequence and within the influence of wave- and storm activity. The depositional environment is envisaged as a shallow water deltaic environment that experienced rapid water level rise associated with a transgression event (Gutzmer et al., 2002). These authors suggest that Mn precipitation was induced by mixing between Mn-bearing surface or sub-surface waters and more alkaline waters in the main basin. Importantly, they also identify a prevalence of biogenic oncoids (coated grains) and suggest a biological influence in the formation of this deposit.

Structure-hosted deposits in the Waterberg Group (younger than the ~2.0 Ga depositional age)

The Waterberg Group hosts several structure-hosted Mn deposits and occurrences which, from desktop evaluation of the Council of Geoscience 1:250 000 mapping series, tend to concentrate in the basal Swaershoek Formation of the Nylstroom Subgroup. These rocks are mapped as medium- to coarse-grained sandstones, pebble sandstone, tuffaceous greywacke, siltstone, shale and conglomerate, representing a delta fan that nonconformably overlies felsic rocks of the Bushveld Complex. Despite their extensive distribution, relatively few descriptions exist for these deposits (De Villiers, 1960; Hammerbeck and Taljaardt, 1976; Callaghan, 1991). In an overview of the economic mineral potential of the Waterberg Group, Eriksson et al. (1997) suggests that the structure-hosted Mn enrichments (vein-fillings and shear zone impregnations) are likely related

to the episodically-activated and long-lived Thabazimbi-Murchison Lineament which has a tectonic history of >2.5 Ga (Good and de Wit, 1997). They also note an anomalous association between Mn and W, tentatively suggesting an involvement of hydrothermal fluids in the enrichment process.

Exhalative-type manganese occurrences in the Namaqua Metamorphic Province (~1.3 to 1.2 Ga)

The Bushmanland Subprovince of the Namaqua Metamorphic Belt hosts a series of polymetallic deposits associated with hydrothermal exhalative processes that occurred between 1 285 ± 14 and 1 198 ± 10 Ma (Cornell et al., 2009). Most notable of these are the sulphide deposits in the Aggeneys-Gamsberg ore district where base metal enrichments are associated with manganiferous ironstones and barite in the pelitic-chemogenic Gams Formation (e.g., Rozendaal et al., 2017). Here, ambient Mn concentrations are generally regarded as having a negative impact on sulphide ore qualities. This is particularly true for the giant Gamsberg Zn ore body where Mn concentrations can reach in excess of 3 wt.% in the sphalerite mineral structure (Schouwstra et al., 2010; McClung and Viljoen, 2011), thus having negative implications for Zn beneficiation by traditional smelting approaches. The latter authors suggest solvent extraction as a means to control Mn concentrations in the Zn product stream, and possibly to generate a saleable Mn by-product. Similar Mn enrichment in sphalerite is also observed at the Big Syncline deposit, which also forms part of the Aggeneys-Gamsberg ore district (Motloba et al., 2024).

Genetically related to the exhalative base metal enrichment, and likely more distal from the vent sites, are a series of Mn occurrences found within the metasedimentary rocks of the Bushmanland Subprovince (Blignault et al., 1983; Strydom and Visser, 1986; Astrup and Tsikos, 1998). Most notable of these is an 8 km long by up to 3.7 m wide zone of mineralisation located on the farm Gams 60. Here, grades are as high as 26 wt.% Mn (Coetzee, 1958; Astrup and Tsikos, 1998) and the ore paragenesis comprises jacobsite, bixbyite, pyrolusite, cryptomelane and psilomelane.

Hydrothermal upgrade of manganese ores in the Kalahari Manganese Field and Postmasburg Manganese Field (~1.2 to 1.0 Ga; 0.6 Ga)

The northern extremity of the KMF was affected by an episode of hydrothermal fluid flow that resulted in stripping of Ca, Mg, CO_2, and SiO_2 from pre-existing Mamatwan-type Mn lutites (Gutzmer and Beukes, 1997b; Chetty and Gutzmer, 2012). This so-called Wessels alteration event (from the homonymous Mn mine) was localised along a series of north-south trending normal faults and affected less than 5% of the preserved area of the KMF (Tsikos et al., 2003). Estimates of the fluid temperature are variable (i.e., from <200° to >400°C; Dixon, 1985; Miyano and Beukes, 1987; Gutzmer and Beukes, 1996b; Lüders et al., 1999), and the age estimates are best constrained by Ar-Ar dates of sugilite (1.04 Ga) and norrishite (1.01 Ga) provided by Gnos et al. (2003), suggesting a temporal linkage to the Kibaran orogeny (Gutzmer and Beukes, 1996b). The resultant alteration mineralogy shows marked zonation from a ferruginised fault zone which grades outwards into a secondary braunite assemblage, then hausmannite-braunite II, then hausmannite-bixbyite, then a braunite II zone, before returning to unaltered Mamatwan-type braunite-kutnohorite mineralogy (Gutzmer and Beukes, 1996b). This alteration resulted in an increase in the ore grade from ~35 to 38% Mn to 45 to 60% Mn and a concomitant decrease in the thickness of the ore bed by around 30% (Gutzmer and Beukes, 1997a). A much later hydrothermal event known as the Mamatwan event affected the KMF and is loosely constrained to ~0.6 Ga (Gutzmer and Beukes, 1996b). The fluid flow during this event was constrained to east-northeast–west-southwest trending joint and fracture sets and is associated with a jacobsite-sulphide-quartz paragenesis replacing Mamatwan-type braunite and hematite assemblages (Gutzmer and Beukes, 1996b).

Alternative suggestions for hydrothermal alteration and upgrading processes in the KMF have been introduced by Tsikos et al. (2003) and later by Tsikos and Moore (2006). The former authors highlight the regional unconformity contact between the Transvaal Supergroup and Olifantshoek Group as a previously underestimated low-angle structural conduit facilitating hydrothermal fluid-flow. This suggestion was based on the development of top-down alteration and metal upgrading effects recorded in the Hotazel strata with increasing distance from the unconformity contact. Further, Tsikos and Moore (2006) report the occurrence of sodic metasomatic mineral assemblages developing in a bedding-parallel fashion at the transitional contacts between BIF and Mn-rich layers of the Hotazel Formation.

Recent work (Fairey et al., 2019) provides renewed support to the hydrothermal origin of the PMF ores, implicating regional scale hydrothermal processes that could have led to the formation of both the Fe and Mn ore deposits of the PMF. The widespread occurrence of alkali-dominated minerals such as armbrusterite, aegirine, sugilite and arsenotokyoite in the matrix of the PMF ores constitutes evidence for the involvement of alkali-rich brines in ore formation. These assemblages are comparable to those observed in the northern KMF (Tsikos and Moore, 2006) and point to at least a causal connection to a common, regional-scale alkali hydrothermal system affecting parts of both the PMF and the KMF. Radiometric Ar-Ar dating of these assemblages places the hydrothermal ore-formation at approximately 620 Ma, thus coinciding with the Mamatwan alteration event mentioned earlier (Moore et al., 2012; Costin et al., 2015; Fairey et al., 2019). However, earlier geochronological work also documented a 1.2 to 1.1 Ga hydrothermal footprint in the PMF, which broadly correlates with the age of the Wessels alteration event (Van Niekerk, 2006). The spatial extent and relative importance of these hydrothermal events within the PMF remain not well constrained.

Supergene enrichment at the African erosional surfaces (~40 to 10 Ma)

Since the early to mid-Cretaceous, the southern African land surface has been affected by at least two distinct periods of uplift and denudation (e.g., Partridge and Maud, 1987; Figure 1b). The

first of these is known as the African land surface and is related to uplift and rifting that occurred during Gondwana break-up in the mid- to late Cretaceous. Further uplift and tilting led to the development of the later post-African 1 land surface, and the onset of this event is variably assigned to ~42 Ma (Gutzmer et al., 2012), ~30 Ma (Burke and Gunnell, 2008) or ~18 Ma (Partridge and Maud, 1987). Climatic conditions at the time of the African land surface and during early formation of the post-African 1 land surface were hot and humid, which will have promoted deep chemical weathering (van Niekerk et al., 1999; Vafeas et al., 2018). Deep weathering ceased around 5 Ma when climatic conditions in South Africa became more arid (Gutzmer et al., 2012).

Supergene enrichment of Kalahari Manganese Field and Postmasburg Manganese Field

Gutzmer and Beukes (1996b) document a supergene alteration event known as the Smartt event, which is poorly constrained in age to between 100 and 10 Ma. The Smartt event is confined to the southern and eastern parts of the KMF where it manifests as oxidation of primary braunite-rich Mamatwan-type ores in normal faults and breccia bodies. Although ten minerals have been identified as the paragenesis of the Smartt event, the major minerals are todorokite and those belonging to the manganomelane group. Another supergene alteration event, possibly associated with the African surface, is known as the Mukulu enrichment event. This has affected the thrusted packages of KMF Wessels-type ore on the farm Mukulu, which is transected by the Blackridge thrust (Vafeas et al., 2018, 2019). The alteration has resulted in As- and V- enrichment in the bulk rock chemistry, along with concomitant precipitation of authigenic fluorapatite (Vafeas et al., 2019). Apatite U/Pb geochronology indicates an age of 77 Ma, representing a discrete (yet likely quite localised) episode of supergene alteration that precedes the main period of supergene alteration that is associated with the post-African 1 erosional surface.

More recent supergene enrichments are associated with the post-African 1 erosional surface, which is locally termed the Kalahari unconformity. Using Ar-Ar dating, Gutzmer et al. (2012) constrained the peak periods of supergene weathering at ~27 Ma, 10.1 Ma and 5.2 Ma. The supergene enrichment primarily affects the Mamatwan-type ores to the east of the KMF, where the mineralogy is represented by microcrystalline and friable todorokite and manganomelane minerals (Gutzmer et al., 2012). The supergene enrichment also results in Mn grades reaching as high as 50 wt.% Mn, where grade is both a function of the proto-ore and depth below the unconformity surface (highest grades closest to the unconformity). Supergene enrichment of Wessels-type ore is less well developed, with minor alteration reported around the area of the Black Rock outcrop. Here, hausmannite has been partially replaced by cryptomelane and replacement is typically restricted to grain boundaries and micro-fractures (Gutzmer and Beukes, 1996b). Earlier workers reported a more extensive range of predominantly Mn^{4+}-bearing minerals including ramsdellite (MnO_2), todorokite, and birnessite, among others (e.g., de Villiers, 1970).

The Postmasburg Mn field has also been affected by recent localised supergene enrichment. Gutzmer (1996) identified the main supergene minerals as cryptomelane and romanechite which formed from downward percolating oxidising meteoric fluids enriched in Ba and K, and deficient in sulphur. Additionally, lithiophorite shows local enrichment particularly where there was excess Al available from weathering of shale-rich lithologies in the Western Belt ores. In the Eastern Belt, De Villiers (1960) reported historical mining of pyrolusite-rich veins which cut down into the underlying dolostones.

Other deposits associated with the African erosion surfaces

The North West Manganese Field (Pharoe et al., 2020; Figure 1) comprises a series of Mn wad deposits including the Ryedale, Houtkoppies, Wes Wits, Klipkuil, General Nice deposits and other smaller occurrences. These deposits are all associated with one of the African erosional surfaces (>18 Ma; Pack et al., 2000), which expresses locally as the deeply weathered Waterval Saprolite unit. The Ryedale and Houtkoppies deposits are anomalous in that they are hosted in Karoo Supergroup rocks and are believed to have formed from weathering of sideritic 'blackband' units (van Niekerk et al., 1999; Pack et al., 2000). The majority of the deposits formed from deep weathering of manganiferous carbonate units of the underlying Neoarchaean Malmani Subgroup dolostones of the Transvaal Supergroup (van Niekerk et al., 1999; Pharoe and Liu, 2018; Pharoe et al., 2020). The Mn enrichments within these settings occur in a variety of different forms including manganocretes, recent Mn wad, transported pedogenic ferromanganese nodules (van Niekerk et al., 1999), and Mn nodules formed in lacustrine settings (Pharoe et al., 2020). Much of the Mn is present as amorphous phases (particularly within the wad), although romanechite, cryptomelane, galaxite and pyrolusite have been documented (Table 3).

The ~55 Ma Zandkopsdrif carbonatite complex is interpreted as the root zone of a carbonatite volcano and comprises a carbonatite-phlogopite breccia, aillikite and transgressive carbonatite dykes (Harper et al., 2015; Ogungbuyi et al., 2022). The complex was deeply weathered during the development of the post-African 1 land surface (Renno et al., 2016; Figure 1b), giving rise to a ~80 m thick supergene cap which includes significant occurrences of Mn as Fe-Mn laterite and manganiferious ferricrete (Harper et al., 2015). Unweathered carbonatite material contains background concentrations (1 to 3 wt.%) of Mn which deports primarily in ankerite. Chemical weathering has upgraded the Mn tenor to an average of 6.9% in the weathered zone, where it occurs primarily as pyrolusite and romanechite (Harper et al., 2015, and reference therein). This Mn concentration may be exploited as a byproduct of rare earth element mining, whereby it can be concentrated as a Mn sulphate product during processing of the targeted monazite ores. Locally, higher grade Mn pockets exist as horizontal accumulations which are interpreted to reflect palaeo groundwater levels, and as sub-vertical vein sets (Harper et al., 2015). Although other weathered carbonatites are known in the region, and indeed elsewhere in South Africa, the low average grade (i.e., 6.9% Mn at Zandkopsdrif) precludes these occurrences as being noteworthy Mn exploration targets.

Recent and ongoing manganese enrichment processes

Cape vein and mound deposits

Manganese occurrences exist in two discrete settings in the Cape Supergroup, viz. as structurally-hosted (and of lesser importance, sandstone replacement) occurrences and as surficial mound-type occurrences associated with manganiferous hot springs (von der Heyden et al., 2024). From an economic standpoint, the structurally-hosted occurrences have received the most attention and have been mined historically at several localities for use in glass-making and in the steel industry (Cole, 2014, and references therein). Although discussed here under a recent enrichment, the age of the structure-hosted occurrences is not well constrained, though they must be younger than their ~400 Ma host quartz arenites (typically Peninsula Formation). A traditional consensus is that these occurrences form from percolating, mildly acidic groundwaters which have the capacity to mobilise background Mn for re-deposition in favourable structural sites (i.e., a lateral secretion model; Marchant et al., 1978; Compton, 2004; McGregor, 2013). More recently, Killick (2020) suggested that replacement processes of saprolitised dykes may be locally important for the Hout Bay deposit from which 5 130 tons of ore was mined in the early 1900's (Cole, 2014). Von der Heyden et al. (2024) posit that whereas small scale Mn occurrences and Mn coatings are ubiquitous within the Cape Supergroup, multiple factors should align to give rise to a more significant Mn mineral deposit. Examples of such factors include favourable fluid characteristics (e.g., warmer temperatures, higher salinity, and older ^{14}C age), focusing of fluid flow in fracture networks and along local aquiclude layers, and near-surface structural trap sites where oxidation takes place by inorganic and/or biologically-mediated processes. The Mn mineralisation often exhibits open-space filling textures, and the dominant minerals that have been recorded include primarily cryptomelane, and psilomelane, pyrolusite, and nsutite (de Villiers, 1960; McGregor, 2013; von der Heyden et al., 2024).

The mound-type Mn occurrences are recorded in at least three localities in the Cape Supergroup (Caledon, Warmwaterberg, Towerwater), and each is intimately associated with a chalybeate hot spring (de Villiers, 1960; von der Heyden et al., 2024). The manganiferous mound material is generally quite friable and comprises poorly crystalline Mn^{4+} minerals, and goethite as the dominant Fe mineral (von der Heyden et al., 2024). These mounds form when warm, relatively chloride-enriched spring fluids discharge via fault conduits at surface, where they are readily cooled and oxidised by atmospheric O_2. Recent work by Von der Heyden et al. (2024) details a high diversity of micro-organisms including several phyla of known Mn-oxidising bacteria associated with these manganiferous spring waters.

Modern pedogenic processes in the Malmani Subgroup dolostones

Highly manganiferous oxisol developed in the soil profile overlying the Malmani Subgroup dolostones on the eastern escarpment of South Africa present a useful case study for understanding the processes that give rise to Mn wad development (Figure 7). The deposits are best developed near to the town Graskop and are mined as raw materials for agricultural Mn sulphate and Mn oxide products (www.bushveldmanganese.com; accessed 18/07/2023). Grades of up to 17% Mn have been reported, with lithiophorite and birnessite identified as the main Mn minerals (Dowding, 2004; Dowding and Fey, 2007), and previous workers additionally identifying todorokite and nsutite (Hawker and Thompson, 1988). Based on textural evidence and chemical evidence, it appears that lithiophorite is the dominant Mn mineral in the lower soil horizons (i.e., directly overlying carbonate regolith), whereas under more acidic and organic-rich conditions in the upper soil profile, lithiophorite is reductively dissolved and Mn repartitions into Mn oxide nodule form (Dowding and Fey, 2007; Figure 7).

Deep marine nodule growth

Deep-marine polymetallic Mn nodules, which predominantly comprise Mn and Fe oxides and oxyhydroxides (Figure 6), continue to attract scientific and economic attention as a low-carbon source for critical metals (e.g., Hein et al., 2020). The occurrence of Mn nodules is well documented off South Africa's coastline where they have been studied since the 1960's (e.g., Willis and Ahrens, 1962; Summerhayes and Willis, 1975; Rogers, 1995; Ovechkina et al., 2021).

Due to the relatively low number of available samples (and difficulty in obtaining samples), mineralogical and chemical data for Mn nodules collected from off South Africa's coastline are relatively sparse (Table 4; SI 1 and Figure 11). Available mineralogical data suggests that todorokite is the dominant mineral phase (Rogers, 1995), although birnessite (δ-MnO_2) and disordered phyllomanganates (e.g., vernadite) may be locally important (Hein et al., 2020). Historical comments on the economic viability of exploiting these nodules require reconsideration given the increased metal prices and decreased cut-off grades of the present day. Any reconsideration, however, would need to take into account the legislative considerations and importantly, the potentially negative environmental implications of sea-bed mining. Previous work, based on measured Co+Cu+Ni concentrations of ~1% (relative to a cut-off grade of 2%) and measured Mn/Fe ratios of <2, Rogers (1995) deemed the evaluated nodules from the southern African coastline as sub-economic. This author further concluded that the best exploration potential is in the Cape Basin (north of 33°S; away from turbulent Agulhas eddies and ice float debris; Figure 11), corroborating data from other studies that highlight the favourable chemistry of nodules from this basin (e.g., Summerhayes and Willis, 1975; Cronan, 1997). Rogers (1995) further suggested a lower prospectivity both in the Mozambique Ridge where bathymetric depths are too shallow to exclude dilution by carbonates, and in Mozambique Basin which may experience contamination by ice float debris in the south and by terrigenous material from the Zambezi deep water fan in the north.

Table 4. Summarised major- and economic element data for manganese (Mn) nodules and crusts sampled near to South Africa's coastlines. Less than sign (<) denotes that only the maximum value is reported (full data table and references in SI 1). (A supplementary data file is archived in the South African Journal of Geology repository (https://doi.org/10.25131/sajg.127.0039.sup-mat)).

Basin	No. samples	Depth (m)	Mn (%)	Fe (%)	Cu (%)	Ni (%)	Co (%)	Zn (%)	Pb (%)	Al_2O_3 (%)	CaO (%)	SiO_2 (%)	P_2O_5 (%)
Atlantic Sector	25	1790 to 5176	0.5 to 26.8	2.8 to 20.9	<0.88	<1.94	<0.70	<1.75	<0.22	2.8 to 3.2	0.8 to 10.1	1.9 to 19.6	<0.5
Indian Sector	80	1260 to 5450	0.2 to 36.5	1.3 to 47.9	<0.90	<1.43	<0.77	<0.58	<0.24	1.1 to 4.2	0.2 to 16.7	3.5 to 44.4	<13.3
Cape Basin	18	3600 to 5230	14.3 to 22.8	3.2 to 15.3	<0.57	<1.07	<0.21	<0.12	<0.11	2.1 to 7.1	1.4 to 3.6		<0.26

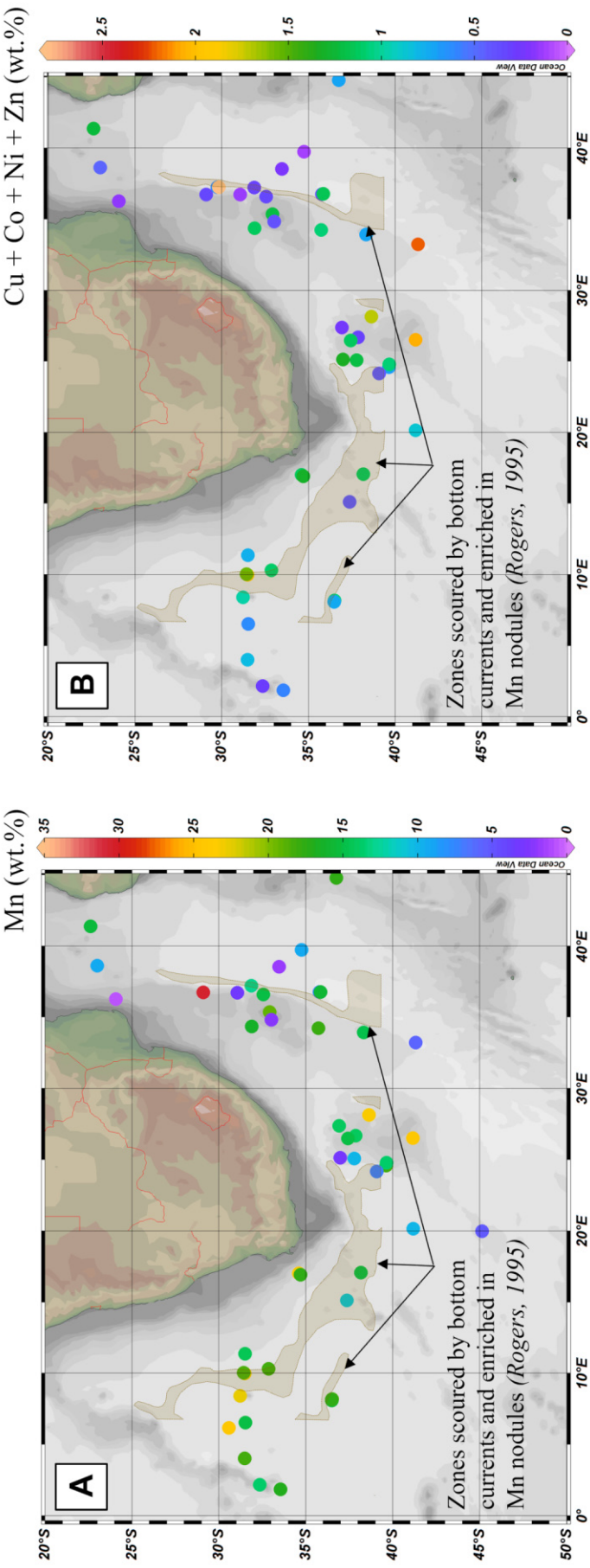

Figure 11. *Distribution of manganese (Mn) nodules sampled from around South Africa's coastline (data from Dutkiewicz et al., 2020) and showing the regions for elevated Mn nodule prospectivity (from Rogers, 1995). (**A**) Measured Mn concentrations in sampled ferromanganese nodules and crusts. (**B**) Total base metal concentrations (Co + Cu + Ni + Zn) in sampled ferromanganese nodules and crusts.*

Geometallurgical implications for South Africa's diverse manganese parageneses

The value of geometallurgy towards maximizing the recovery and use of Mn ore bodies is increasingly being appreciated and applied. Although there are several definitions of geometallurgy in the literature, it is best understood as a cross-disciplinary approach that incorporates geology, mine planning, metallurgy, and geostatistics to maximise the value of mining operations (e.g., Lund and Lamberg, 2014; Dominy et al., 2018). Geometallurgical activities are underpinned by a detailed understanding of the primary and secondary variables that impact mining efficiencies and performance. These performances can be measured by net present value, sustainability or various operational metrics. Measurement of primary variables is a staple of mining operations; for example, the grade variable has traditionally informed the definition of value in Mn operations. The primary market for Mn products, which is the ferroalloy industry, still dictates grade as the primary variable for quality control. However, modern understanding of process mineralogy has established the importance of secondary and derived variables. For example, there is increasing emphasis on the recovery of the value mineral (Table 2), rather than elemental (Mn) recovery, as this may be more meaningful towards optimising the mining value chain.

Process mineralogy of Mn ores considers the mineralogy and mineral chemistry alongside parameters such as texture and microporosity of particles. South African Mn ores encompass a diverse array of oxide/oxyhdroxide, carbonate, silica-bearing and ferruginous Mn minerals, which vary both between deposits and spatially within individual deposits (Table 3). These minerals exhibit other variations, including their associations with gangue minerals, incorporation of trace elements, and the Mn valence state. Beneficiation and extraction process design and process operation are highly dependent on these secondary variables, which further impact considerations such as the downstream environmental concerns (Peterson et al., 2021). Although detailed mineralogical understanding is crucial towards optimised Mn geometallurgy, the situation is even more nuanced given that ore particles (not discrete or distinct chemical species or mineral species) are the unit inputs to processes (Clout, 2003). In this context, particle texture refers to the size, shape, and relative arrangement of the constituent mineral grains/crystals in the particle, as well as the size, shape, and relative arrangement of any pore space present (Lishchuk et al., 2015; Peterson et al., 2021).

Current beneficiation strategies and future opportunities

Historically mined Mn ores, particularly those from the northern KMF, have typically been high-grade material requiring limited beneficiation to achieve market specifications. High-grade ores (e.g. Wessels-type ores, >45% Mn) do not require involved beneficiation, and the processing is thus limited to ore dressing. This ore dressing involves crushing, washing and screening into the relevant particle sizes that are considered optimal for the client (predominantly ferroalloy smelters; e.g., Chetty, 2010; Dworzanowski, 2013; Steenkamp and Basson, 2013; Chetty and Gutzmer, 2018; Chetty et al., 2023). Fine material generated from these Mn ores can be agglomerated through sintering to produce suitable furnace products. Sintering can improve the physical and chemical properties of ore, specifically fine material, such as its strength, reducibility, and resistance to degradation during transportation and handling (Pienaar and Smith, 1992). It can also help to remove volatile impurities and improve the homogeneity of the ore for subsequent smelting processes. Particle size modification provides operational and logistical advantages (Krogerus et al., 2013), particularly given that 'lump' products (6 to 75 mm diameter) are financially incentivised.

The limitations of lower grade Mn ores, particularly for the ferroalloy market, is the small grain size of Mn minerals within the ore (which would result in small particle sizes if liberated); and high content of gangue, including siliceous gangue, Fe-bearing minerals and minerals containing Al and P (penalty elements in steel manufacture). Elsewhere, and at laboratory test scale, low-grade material has been beneficiated through the application of gravity methods, such as spirals and jigs, and dense media separation has also been utilised to separate coarse-grained or physically separable particles of Mn from siliceous gangue and Fe-bearing minerals (Table 5; Pienaar and Smith, 1992; Eric, 1995; Steenkamp et al., 2020). Mamatwan-type ores are typically upgraded using dense media separation which is improved in performance by combining the process with gravity separation using hydrocyclones (Pienaar and Smith, 1992). Through extended beneficiation, opportunities exist to exploit lower grade Mn ores, which are currently overlooked due to higher infrastructure investment implications. Exploitation of higher Fe content ores or ferruginous ores in which Mn and Fe cannot be physically separated include, fine griding, roasting of ores, and high intensity magnetic separation (wet or dry) (Mpho et al., 2013; Kivinen et al., 2010; Steenkamp et al., 2018; Singh et al., 2020; Steenkamp et al., 2020; Elliot and Barati, 2020). Table 2 shows that a number of Mn minerals are paramagnetic and can be recovered using direct magnetic separation. However, this process has been found to be less efficient for separation of Mn and Fe minerals and more successful for separation of Mn from siliceous gangue (Table 5; Elliot and Barati, 2020). Froth flotation is a less common beneficiation process and has proven applicability to oxide and carbonate Mn ores, particularly those containing pyrolusite. This technique is capable of removing calcareous and aluminosilicate gangue, but is typically ineffectual at upgrading the Mn/Fe ratio (Singh et al., 2020, and references therein).

Impacts of geometallurgical characteristics for ferroalloy production

Manganese ferroalloys are produced from smelting in either submerged arc furnaces, electric arc furnaces or blast furnaces (Figure 2). Primary production of Mn is achieved by the reduction of Mn minerals by coke, which is the primary

reductant. Smelters are high energy consumers and require strict and careful control for environmental, safety and efficient process control. A careful charge of feed, which includes the Mn ore, the reductant (coke) and the relevant fluxes, is required to maintain steady state conditions within the smelter. High temperatures are maintained in the furnace and the separation and removal of impurities from the Mn product is achieved by effective fluxes. Silica is a particularly important flux since this maintains slag fluidity and prevents precipitation of Mn losses through the formation of phases such as Mn spinel in the slag. Manganese minerals containing silica and natural fluxing gangue are termed self-fluxing ores (Tathavadkar et al., 2010; O' Shaughnessy et al., 2004).

The reaction pathways to the formation of Mn in the product phase in the reaction zone of the smelter are dependent on the mineralogy of ore charged into the smelter. For example, the bixbyite reduction pathway is less endothermic than the hausmannite reduction pathway (Chetty and Gutzmer, 2018). Whilst it is suggested that the bixbyite pathway can be less energy intensive than the hausmannite, more oxygen is evolved in the process and a higher reductant charge is thus required to drive off the oxygen. In addition, the excess oxygen may facilitate rising temperatures in the smelter due to the exothermic combustion of CO gases produced from coke (Tathavadkar et al., 2010). Ultimately higher oxidation states (e.g., Mn^{4+}) in the Mn mineral yield a longer reduction pathway that places a burden on reductant.

Carbonate minerals decompose thermally in a reducing environment to form MnO and CO_2 gas (calcination process). The formation of MnO has the advantage of requiring less reductant (in the form of C) to further reduce the species to Mn, compared to naturally occurring oxide minerals. However, heat is required to facilitate the initial carbonate decomposition step (O' Shaughnessy et al., 2004). Careful blending of carbonates with oxide ores reduces excess C utilisation in a smelter producing SiMn, although a balanced Si:Mn ratio in both ores is required (O' Shaughnessy et al., 2004). Decreasing fine carbonate minerals in low grade ores is possible through beneficiation followed by sintering to produce a structurally sound smelter product. The heat provided from the sintering/agglomeration processes has the additional advantage of facilitating decomposition of the mineral to MnO, which is then ready for smelting.

From a geometallurgical perspective, a narrower classification of the smelter feed is of clear value to the smelter efficiency and thus to the business. To achieve more efficient furnace optimisation, blending control is already implemented. However, this is based predominantly on grade and chemical variables. Opportunity exists though to be even more efficient with a narrower product distribution, based on feed mineralogy. The grade metric is already a control variable in mining and to achieve mineralogical control in mining, it is necessary to characterise the ores accordingly. Towards this end, the geometallurgical approach of Chetty (2010) demonstrates how X-ray diffraction provides detailed mineralogical characterisation, which in turn can inform furnace optimisation.

Table 5. Mineral processing and geometallurgical considerations associated with the broad manganese (Mn) ore categories.

Ore category	Grade	Typical mineralogy	Selected RSA examples	Ore dressing	Beneficiation	Geometallurgical considerations
Hypogene upgrade of Mn protolith	High grade oxide ores	Hausmannite, bixbyite, braunite II	KMF Wessels type; upgraded PMF ores	Crushing and screening	Not required	Maximise lump to fine ratio
Primary chemical sedimentation and ancient supergene enrichments	Low grade: oxide-carbonate-silicate	Braunite, kutnohorite	KMF Mamatwan type; low grade PMF ores (eastern belt)		Dense media separation, Gravity separation (jigging, spirals), direct magnetic seperation	Minimise siliceous gangue, upgrade Mn content
Ancient supergene enrichments	Low grade: ferruginous	Braunite, bixbyite, pyrolusite	PMF eastern belt ores		Roasting (C, CO/CO_2), magnetic separation	Upgrade Mn/Fe ratio, minimisation of Fe gangue
Recent supergene	Low grade: high valence Mn oxides	Manganomelane minerals, pyrolusite	NWMF		Dense media separation, gravity separation, flotation (uncommon)	Minimise Si and Fe gangue, P content commonly detrimental, reductants required in downstream processing (except when Mn required as oxidising agent (chemicals industry))
Mn nodules	Low grade: not currently exploited	Poorly crystalline Mn phases	Deep ocean sea-floor		Advanced hydrometallurgy or pyrometallurgy	Fine intergrowths of Fe and Mn, complete destruction required. Grade of sweetener elements Co, Cu, Ni, Zn important.

Beneficiation and extraction of manganese minerals for alternative markets

One of the fastest growing markets for Mn is the battery manufacture industry, which is driven by the global zero C targets that are motivating the battery storage business. Lithium Mn oxide (LMO) and Ni-Mn-Co (NMC) technologies are two important types of Li-ion battery, with each crucially requiring the presence on Mn in the cathode structure. Due to its non-controversial accessibility compared to conflict-associated metals such as cobalt, research is focused on development of large-scale batteries based on Mn alone. Chemical Mn dioxide (CMD), electrolytic Mn (EM) or electrolytic Mn dioxide (EMD) are all products of hydrometallurgical processing of Mn ores. A common precursor to these is Mn^{2+} sulphate, which is produced from sulfuric acid leaching of Mn minerals. Manganese sulphate is also used for fertiliser production and as a component in dyes and pigments, among other Mn end-uses (Zhang and Cheng, 2007).

Hydrometallurgical operations include indirect or direct leaching approaches. Indirect leaching entails pre-reduction processes, such as roasting, in order to reduce high valence minerals to lower valencies that are more amenable to leaching. Direct hydrometallurgical production involves reductive leaching to form Mn products, in the form of metallic Mn or metal powders (e.g., Mn sulphate). The fundamental process is the reduction of Mn from high oxidation states (+4, +3) to a low oxidation state (+2), with the use of a suitable reductant. Reductive leaching can employ a range of reductants including Fe^{2+}, various C sources (including organics), and hydrogen peroxide, amongst others (Sinha and Purcell, 2019; Jiang et al., 2004; Nayl et al., 2011). Manganese carbonate minerals are most easily leached and offer the advantage of comprising Mn in its divalent state (Addai et al., 2016). The carbonate anion has the dual advantage of behaving as a reducing agent for other Mn minerals such as pyrolusite (Addai et al., 2016).

The higher valence oxyhydroxide and oxide minerals are more difficult to leach and require a reducing agent. These minerals find application in the chemicals industry where, for example, pyrolusite-rich ore is a preferred feed for the manufacture of K permanganate ($KMnO_4$), an industrial oxidising agent. This is because Mn is already in an oxidised valence state and because its mineral structure (small tunnel cross-sections (Newton and Kwon, 2020)) ensures limited uptake of extraneous ions, thus ensuring a relative degree of chemical purity. Other higher valence, but larger tunnel-structured Mn minerals (cryptomelane, hollandite, romanechite and todorokite) take up ions such as K^+, Ba^{2+} and Mg^{2+} and other elements, and are thus less viable as starting material to form high purity products. Instead, because of their larger tunnel structures, these and the layered Mn oxides (e.g., birnessite), are commonly used in environmental remediation (e.g., reactive barriers) because of the high adsorption capacity for, e.g., heavy metals and metalloids (e.g., Li et al., 2021). Other documented uses of higher oxidation state Mn ores from South Africa include the use of wad-type supergene ores from the North West Manganese Field as a natural oxidant for U recovery from mining in the Witwatersrand basin (Pack et al., 2000), and consideration of natural nsutite from the same area as an early battery material (Ortlepp, 1964).

Conclusions

Manganese enrichments in South Africa span a diverse array of genetic models and geological settings. The most important of these is the chemical sedimentation that took place in the KMF at and just prior to the GOE. This gave rise to the world's largest on-land accumulation of Mn, the bulk of which comprises Mamatwan-type braunite (mixed valence silica-bearing oxide) and kutnohorite (divalent carbonate) mineralogy. At least 3% of the total KMF Mn reserve has been upgraded by later hydrothermal fluid flow to render a high-grade Wessels-type ore. The mineralogy of this ore is variable and controlled by the extent of fluid-wall-rock interaction, resulting in $Mn^{2+/3+}$ oxide assemblages (i.e., haussmanite, bixbyite) in the highest grade zones proximal to the structural feeder conduits which grade progressively back into the Mamatwan-type proto-ore. The second-most important mechanism for Mn enrichment is through both palaeo- and more recent supergene alteration processes operating particularly on lithologies containing Mn-bearing carbonates (e.g. dolomites, carbonatites). Although this results in a Mn^{4+} dominated mineral assemblage (manganomelane, pyrolusite, lithiophorite, etc.), for the PMF deposits (~2.5 Ga host rock upgraded at ~2 Ga and ~1 Ga) the mineralogy has matured into mixed-valence braunite, and trivalent partridgeite and bixyite parageneses. Structurally-controlled Mn enrichments are prevalent particularly in fractured quartzite units and typically comprise low grade, and P-rich assemblages of Mn^{4+} minerals.

The diversity of the Mn mineralogy associated with each genetic model and with each individual deposit has strong geometallurgical implications. The main end use for Mn is in steelmaking, where reduced Mn^{2+} minerals are favoured since they do not require excessive reduction in the furnace environment. This impacts the energy considerations and decreases the amount of coke required as a reducing agent, thus also minimising the amount of CO_2 emissions arising during smelting. In the increasingly important battery production sector, mineralogy inherently affects the processing routes, costs and efficiencies as the raw feed is transformed into battery precursor material Mn^{2+} sulphate. Although important contributions have been made to the geometallurgy of RSA Mn ores (e.g., Chetty, 2010; Bussin, 2022), there exists vast scope to further develop this field using detailed understanding of Mn mineralogy and textures as key parameters that impact mining, beneficiation and saleability. Such detailed mineral-level understanding also holds implications the exploration paradigms employed for discovery of new deposits, and for the important field of medical geology (e.g., Duka et al., 2011), where the relative adversity (ecotoxicology and toxicology to human health) of each different Mn mineral is not currently constrained.

Acknowledgments

The authors would like to acknowledge the researchers upon whose work this review has been built. Particularly, we acknowledge the massive contribution made by the late Prof Nic Beukes whose efforts meaningfully advanced the status of knowledge on this broad subject matter. This review paper is dedicated to his memory. We thank Dr A. Dutkiewicz for sharing the dataset on Mn nodule chemistry, and P. Miller for his RSA Mn mining cadastre. Prof B. Cairncross is thanked for supplying the high-quality images of various Mn ore minerals. We further thank the reviewers V. Oge, J. Gutzmer, B. Maynard and two anonymous reviewers, the handling editor M. Elburg, and G. Henry and L. Vonopartis for feedback and editorial assistance that served to strengthen the final version of this manuscript. Financial support is acknowledged from DSI-NRF CIMERA (BvdH, AJBS), as well as from the African Rainbow Minerals Chair in Geometallurgy (BvdH, CD, LvE, MT).

References

Aasly, K. and Ellefmo, S., 2014. Geometallurgy applied to industrial minerals operations. Mineralproduksjon, 5, A21-A34.

Addai, E.K., Acquah, F., Yeboah, I. and Addo, A., 2016. Reductive leaching of blended manganese carbonate and pyrolusite ores in sulphuric acid. International Journal of Mining and Mineral Engineering, 7, 18-36.

Albut, G., Babechuk, M.G., Kleinhanns, I.C., Benger, M., Beukes, N.J., Steinhilber, B., Smith, A.J.B., Kruger, S.J. and Schoenberg, R., 2018. Modern rather than Mesoarchaean oxidative weathering responsible for the heavy stable Cr isotopic signatures of the 2.95 Ga old Ijzermijn iron formation (South Africa). Geochimica et Cosmochimica Acta, 228, 157-189.

Albut, G., Kamber, B.S., Brüske, A., Beukes, N.J., Smith, A.J. and Schoenberg, R., 2019. Modern weathering in outcrop samples versus ancient paleoredox information in drill core samples from a Mesoarchaean marine oxygen oasis in Pongola Supergroup, South Africa. Geochimica et Cosmochimica Acta, 265, 330-353.

Aleksandrov, S.V., Hulka, K., Stepashin, A.M. and Morozov, Y.D., 2005. Effect of manganese and niobium on the properties of low-alloy steels. Metal Science and Heat Treatment, 47, 497-501.

Anacleto, N., Ostrovski, O. and Ganguly, S., 2004. Reduction of manganese ores by methane-containing gas. Iron and Steel Institute of Japan International, 44, 1615-1622.

Astrup, J. and Tsikos, H., 1998. Manganese. In: M.J. Wilson and C.R. Anhaeusser. (Editors), Mineral Resources of Southern Africa. Council for Geoscience, Pretoria, South Africa, 450-460.

Bao, W., Shen, H., Zhang, Y., Qian, C., Cui, D., Xia, J., Liu, H., Guo, C., Yu, F., Li, J. and Sun, K., 2024. Rejuvenating manganese-based rechargeable batteries: fundamentals, status and promise. Journal of Materials Chemistry A, 12, 8617-8639.

Bau, M., Romer, R.L., Lüders, V. and Beukes, N.J., 1999. Pb, O, and C isotopes in silicified Mooidraai dolomite (Transvaal Supergroup, South Africa): implications for the composition of Paleoproterozoic seawater and `dating' the increase of oxygen in the Precambrian atmosphere. Earth and Planetary Science Letters, 174, 43-57.

Bekker, A., Holland, H.D., Wang, P.-L., Rumble III, D., Stein, H.J., Hannah, J.L., Coetzee, L.L. and Beukes, N.J., 2004. Dating the rise of atmospheric oxygen. Nature, 427, 117-120.

Beukes, N.J., 1983. Palaeoenvironmental setting of iron-formations in the depositional basin of the Transvaal Supergroup, South Africa. In: Developments in Precambrian Geology Vol. 6, Elsevier, 131-198.

Beukes, N.J. and Cairncross, B., 1991. A lithostratigraphic-sedimentological reference profile for the Late Archaean Mozaan Group, Pongola Sequence: application to sequence stratigraphy and correlation with the Witwatersrand Supergroup. South African Journal of Geology, 94, 44-69.

Beukes, N.J., Dorland, H., Gutzmer, J., Nedachi, M. and Ohmoto, H., 2002. Tropical laterites, life on land, and the history of atmospheric oxygen in the Paleoproterozoic. Geology, 30, 491-494.

Beukes, N.J., Gutzmer, J. and Mukhopadhyay, J., 2003. The geology and genesis of the high-grade hematite iron ore deposits of the Postmasburg manganese field, South Africa. Applied Earth Science: Transactions of the Institutions of Mining and Metallurgy Section B, 112, 26-30.

Beukes, N.J., Swindell, E.P. and Wabo, H., 2016. Manganese deposits of Africa. Episodes Journal of International Geoscience, 39, 285-317.

Blignault, H.J., Van Aswegen, G., Van der Merwe, S.W. and Colliston, W.P., 1983. The Namaqualand geotraverse and environs: part of the Proterozoic Namaqua mobile belt.

Brookins, D.G., 1988. Eh-pH diagrams for geochemistry. Springer-Verlag, Berlin. 176pp

Bühn, B., Stanistreet, I.G. and Okrusch, M., 1992. Late Proterozoic outer shelf manganese and iron deposits at Otjosundu (Namibia) related to the Damaran oceanic opening. Economic Geology, 87, 1393-1411.

Burke, K. and Gunnell, Y., 2008. The African erosion surface: a continental-scale synthesis of geomorphology, tectonics, and environmental change over the past 180 million years. Geological Society of America, 201. doi: 10.1130/2008.1201

Bussin, D., 2022. A characterization and process mineralogical assessment of the karst-hosted manganese ore deposits at Paling exploration camp in the Postmasburg Manganese Field, Northern Cape Province, South Africa. Unpublished M.Sc. thesis, University of Johannesburg, South Africa, 153pp

Cairncross, B., Beukes, N. and Gutzmer, J., 1997. The Manganese Adventure: The South African Manganese Fields. Associated Ore and Metal Corporation Limited, 236pp

Cairncross, B. and Beukes, N.J., 2013. The Kalahari Manganese Field. Struik Nature, Cape Town, 384pp

Cairncross, B., 2024. Postmasburg Manganese Field, Northern Cape Province, South Africa. Rocks & Minerals, 99, 208-235.

Callaghan, C.C., 1997. The geology of the Waterberg Group in the southern portion of the Waterberg basin. Unpublished M.Sc. thesis, University of Pretoria, South Africa, 164pp

Calvert, S.E. and Pedersen, T.F., 1996. Sedimentary geochemistry of manganese; implications for the environment of formation of manganiferous black shales. Economic Geology, 91, 36-47.

Cape Minerals, 2024. The Kalahari Manganese Field. Available at: www.capeminerals.co.za Accessed 01/07/2024.

Chetty, D., 2010. A geometallurgical evaluation of the ores of the northern Kalahari Manganese Deposit, South Africa. Ph.D. thesis, University of Johannesburg, South Africa, 386pp

Chetty, D. and Gutzmer, J., 2012. REE redistribution during hydrothermal alteration of ores of the Kalahari Manganese Deposit. Ore Geology Reviews, 47, 126-135.

Chetty, D. and Gutzmer, J., 2018. Quantitative mineralogy to address energy consumption in smelting of ores from the Kalahari Manganese Field, South Africa. Proceedings of the 15th International Ferro-Alloys Congress, Cape Town, South Africa, 25-28.

Chetty, D., Nwaila, G.T. and Xakalashe, B., 2023. Fire and water: geometallurgy and extractive metallurgy. Elements, 19, 365-370.

Christianson, D., 2024. South Africa's Manganese Industry. Available at: www.miningdecisions.com. Accessed 01/07/2024.

Clout, J.M.F., 2003. Upgrading processes in BIF-derived iron ore deposits: implications for ore genesis and downstream mineral processing. Applied Earth Science, 112, 89-95.

Coetzee, C.B., 1958. Manganiferous iron ore, hematite, barite, and sillimanite on Gams (portion 1), Namaqualand. Bulletin 28, Union of South Africa, Department of Mines, Geological Survey, 25pp

Coetzee, L.L., Gutzmer, J., Smith, A.J.B. and Beukes, N.J., 2024. Mineralogy and mineral paragenesis of the Palaeoproterozoic manganese ores of the Avontuur deposit of the Kalahari Manganese Field, South Africa. South African Journal of Geology, 127, 31-54.

Cole, D.I., Ngcofe, L. and Halenyane, K., 2014. Mineral commodities in the Western Cape Province, South Africa. Council for Geoscience, Western

Cape Regional Office, Report 12, 90pp
Compton, J.S., 2004. The rocks and mountains of Cape Town. Juta and Company Ltd, 112pp
Corathers, L.A. and Petrican, O., 2005. US Manganese in June 2005. Mineral Industry Surveys, Manganese, 1-7.
Cornell, D.H. and Schütte, S.S., 1995. A volcanic-exhalative origin for the world's largest (Kalahari) manganese field. Mineralium Deposita, 30, 146-151.
Cornell, D.H., Pettersson, A., Whitehouse, M.J. and Scherstén, A., 2009. A new chronostratigraphic paradigm for the age and tectonic history of the Mesoproterozoic Bushmanland ore district, South Africa. Economic Geology, 104, 385-404.
Costin, G., Fairey, B., Tsikos, H. and Gucsik, A., 2015. Tokyoite, As-rich tokyoite, and noélbensonite: new occurrences from the Postmasburg manganese field, Northern Cape Province, South Africa. Canadian Mineralogist, 53, 981-990.
Crerar, D.A. and Barnes, H.L., 1974. Deposition of deep-sea manganese nodules. Geochimica et Cosmochimica Acta, 38, 279-300.
Cronan, D.S., 1977. Deep-sea nodules: distribution and geochemistry. In: Elsevier Oceanography Series Volume 15. Elsevier. 11-44.
Czaja, A.D., Johnson, C.M., Roden, E.E., Beard, B.L., Voegelin, A.R., Nägler, T.F., Beukes, N.J. and Wille, M., 2012. Evidence for free oxygen in the Neoarchean ocean based on coupled iron-molybdenum isotope fractionation. Geochimica et Cosmochimica Acta, 86, 118-137.
Davies, J., Tangstad, M., Schanche, T.L. and Du Preez, S.P., 2023. Pre-reduction of united manganese of Kalahari ore in CO/CO_2, H_2/H_2O, and H_2 atmospheres. Metallurgical and Materials Transactions B, 54, 515-535.
Daye, M., Klepac-Ceraj, V., Pajusalu, M., Rowland, S., Farrell-Sherman, A., Beukes, N.J., Tamura, N., Fournier and G., Bosak, T., 2019. Light-driven anaerobic microbial oxidation of manganese. Nature, 576, 311-314.
De Villiers, J.E., 1944. The origin of the iron and manganese deposits in the Postmasburg and Thabazimbi areas. Transactions of the Geological Society of South Africa, 47, 123-135.
De Villiers, J., 1960. The manganese deposits of the Union of South Africa: Geological Survey of South Africa, Handbook 2, 280pp
De Villiers, P.R., 1970. The geology and mineralogy of the Kalahari manganese-field north of Sishen, Cape Province. Memoir of the Geological Survey of South Africa, 59, 84pp
Diem, D. and Stumm, W., 1984. Is dissolved Mn^{2+} being oxidized by O_2 in absence of Mn-bacteria or surface catalysts? Geochimica et Cosmochimica Acta, 48, 1571-1573.
Dixon, R.D., 1985. Sugilite and associated minerals from Wessels mine, Kalahari manganese field. South African Journal of Geology, 88, 11-17.
Dominy, S.C., O'Connor, L., Parbhakar-Fox, A., Glass, H.J. and Purevgerel, S., 2018. Geometallurgy – A route to more resilient mine operations. Minerals, 8, 560.
Dorr, J.V.N., II, Crittenden, M.D., Jr. and Worl, R.G., 1973. Manganese. In: D.A. Brobst, and W.P. Pratt. (Editors), United States Mineral Resources: U.S. Geological Survey Professional Paper 820, 385-399.
Dowding, C.E., 2004. Morphology, mineralogy and surface chemistry of manganiferous oxisols near Graskop, Mpumalanga Province, South Africa. Unpublished M.Sc. Thesis, University of Stellenbosch, South Africa, 118pp
Dowding, C.E. and Fey, M.V., 2007. Morphological, chemical and mineralogical properties of some manganese-rich oxisols derived from dolomite in Mpumalanga province, South Africa. Geoderma, 141, 23-33.
Duka, Y.D., Ilchenko, S.I., Kharytonov, M.M. and Vasylyeva, T.L., 2011. Impact of open manganese mines on the health of children dwelling in the surrounding area. Emerging Health Threats Journal, 4, 7110.
Dutkiewicz, A., Judge, A. and Müller, R.D., 2020, Environmental predictors of deep-sea polymetallic nodule occurrence in the global ocean: Geology, 48, 293–297. doi: 10.1130/G46836.1
Dworzanowski, M., 2013. The role of metallurgy in enhancing beneficiation in the South African mining industry. Journal of the Southern African Institute of Mining and Metallurgy, 113, 677-680.
Eickmann, B., Hofmann, A., Wille, M., Bui, T.H., Wing, B.A. and Schoenberg, R., 2018. Isotopic evidence for oxygenated Mesoarchaean shallow oceans. Nature Geoscience, 11, 133-138.
Elliott, R. and Barati, M., 2020. A review of the beneficiation of low-grade manganese ores by magnetic separation. Canadian Metallurgical Quarterly, 59, 1-16.
Eric, R.H., 1995. An overview on manganese alloy production and related fundamental research in South Africa. Mineral Processing and Extractive Metallurgy Review, 15, 191-200.
Eriksson, P.G., Reczko, B.F.F. and Callaghan, C.C., 1997. The economic mineral potential of the mid-Proterozoic Waterberg Group, northwestern Kaapvaal craton, South Africa. Mineralium Deposita, 32, 401-409.
Fairey, B.J., Timmerman, M.J., Sudo, M. and Tsikos, H., 2019. The role of hydrothermal activity in the formation of karst-hosted manganese deposits of the Postmasburg Mn field, Northern Cape Province, South Africa. Minerals, 9, 408.
Farquhar, J., Bao, H. and Thiemens, M., 2000. Atmospheric influence of Earth's earliest sulfur cycle. Science, 289, 756-759.
Faure, G., 1986. Principles of isotope geology. Wiley, New York, USA. 589pp
Force, E.R. and Maynard, J.B., 1991. Manganese: syngenetic deposits on the margins of anoxic basins. Reviews in Economic Geology, 5, 147-156.
Freeman, K.H., 2001. Isotopic biogeochemistry of marine organic carbon. Reviews Mineralogy and Geochemistry, 43, 579-605.
Gammons, C.H. and Seward, T.M., 1996. Stability of manganese (II) chloride complexes from 25 to 300 C. Geochimica et Cosmochimica Acta, 60, 4295-4311.
Goa, K., Sun, C. and Wang, Z., 2024. Recent advances in high-performance lithium-rich manganese-based materials for solid-state lithium batteries. Materials Chemistry Frontiers. 1-24. doi: 10.1039/d4qm00513a
Garcia, V.H., Reiners, P.W., Shuster, D.L., Idleman, B. and Zeitler, P.K., 2018. Thermochronology of sandstone-hosted secondary Fe-and Mn-oxides near Moab, Utah: Record of paleo-fluid flow along a fault. Geological Society of America Bulletin, 130, 93-113.
Gholami, A., Asgari, K., Khoshdast, H. and Hassanzadeh, A., 2022. A hybrid geometallurgical study using coupled Historical Data (HD) and Deep Learning (DL) techniques on a copper ore mine. Physicochemical Problems of Mineral Processing, 58, 147841.
Gilkes, R.J. and McKenzie, R.M., 1988. Geochemistry and mineralogy of manganese in soils. In Manganese in Soils and Plants: Proceedings of the International Symposium on 'Manganese in Soils and Plants'. Dordrecht: Springer Netherlands.
Gnos, E., Armbruster, T. and Villa, I.M., 2003. Norrishite, $K(Mn_2^{3+},Li)\ Si_4O_{10}(O)_2$, an oxymica associated with sugilite from the Wessels Mine, South Africa: Crystal chemistry and ^{40}Ar-^{39}Ar dating. American Mineralogist, 88, 189-194.
Godfrey, L.V. and Falkowski, P.G., 2009. The cycling and redox state of nitrogen in the Archaean ocean. Nature Geoscience, 2, 725-729.
Good, N. and De Wit, M.J., 1997. The Thabazimbi-Murchison lineament of the Kaapvaal craton, South Africa: 2700 Ma of episodic deformation. Journal of the Geological Society, 154, 93-97.
Gumsley, A.P., Chamberlain, K.R., Bleeker, W., Söderlund, U., De Kock, M.O., Larsson, E.R. and Bekker, A., 2017. Timing and tempo of the Great Oxidation Event. Proceedings of the National Academy of Sciences, 114, 1811-1816.
Gutzmer, J., 1996. Genesis and alteration of the Kalahari and Postmasburg manganese deposits, Griqualand West, South Africa. Unpublished Ph.D. thesis, University of Johannesburg, South Africa, 490pp
Gutzmer, J. and Beukes, N.J., 1995. Fault-controlled metasomatic alteration of early Proterozoic sedimentary manganese ores in the Kalahari Manganese Field, South Africa. Economic Geology, 90, 823-844.
Gutzmer, J. and Beukes, N.J., 1996a. Karst-hosted fresh-water Paleoproterozoic manganese deposits, Postmasburg, South Africa. Economic Geology, 91, 1435-1454.
Gutzmer, J. and Beukes, N.J., 1996b. Mineral paragenesis of the Kalahari manganese field, South Africa. Ore Geology Reviews, 11, 405-428.
Gutzmer, J. and Beukes, N.J., 1997a. Effects of mass transfer, compaction and secondary porosity on hydrothermal upgrading of Paleoproterozoic sedimentary manganese ore in the Kalahari manganese field, South Africa. Mineralium Deposita, 32, 250-256.
Gutzmer, J. and Beukes, N.J., 1997b. Mineralogy and mineral chemistry of oxide-facies manganese ores of the Postmasburg manganese field, South

Africa. Mineralogical Magazine, 61, 213-231.

Gutzmer, J., Schaefer, M.O. and Beukes, N.J., 2002. Red bed-hosted oncolitic manganese ore of the Paleoproterozoic Soutpansberg Group, Bronkhorstfontein, South Africa. Economic Geology, 97, 1151-1166.

Hammerbeck, E.C.I. and Taljaardt, J.J., 1976. Manganese. In: C.B. Coetzee (Editor), Mineral Resources of the Republic of South Africa, 5th Ed., 167-172.

Harper, F., Wiid, G., Siegfried, P., Brown, J., Hall, M., Njowa, G., Vivier, J., Zietsman, R. and Duke, V., 2015. National Instrument 43-101 Independent Technical Report on the Results of a Preliminary Feasibility Study on the Zandkopsdrift Rare Earth Element and Manganese by-Product Project in the Northern Cape Province of South Africa Independent Pre-Feasibility Study Prepared for Frontier Rare Earths Limited.

Hawker, L.C. and Thompson, J.G., 1988. Weathering sequence and alteration products in the genesis of the Graskop manganese residua, Republic of South Africa. Clays and Clay Minerals, 36, 448-454.

Hein, J.R., Koschinsky, A. and Kuhn, T., 2020. Deep-ocean polymetallic nodules as a resource for critical materials. Nature Reviews Earth & Environment, 1, 158-169.

Hein, J.R., Mizell, K., Koschinsky, A. and Conrad, T.A., 2013. Deep-ocean mineral deposits as a source of critical metals for high-and green-technology applications: Comparison with land-based resources. Ore Geology Reviews, 51, 1-14.

Hem, J.D., 1972. Chemical factors that influence the availability of iron and manganese in aqueous systems. Geological Society of America Bulletin, 83, 443-450.

Henkel, J.V., Dellwig, O., Pollehne, F., Herlemann, D.P.R., Leipe, T. and Schulz-Vogt, H.N., 2019. A bacterial isolate from the Black Sea oxidizes sulfide with manganese(IV)oxide. Proceedings of the National Academy of Science, 116, 12153-12155.

Hodgskiss, S.W. and Sperling, E.A., 2022. A prolonged, two-step oxygenation of Earth's early atmosphere: Support from confidence intervals. Geology, 50, 158-162.

Holland, H.D., 2002. Volcanic gases, black smokers, and the Great Oxidation Event. Geochimica et Cosmochimica Acta, 66, 3811-3826.

Hummer, D.R., Golden, J.J., Hystad, G., Downs, R.T., Eleish, A., Liu, C., Ralph, J., Morrison, S.M., Meyer, M.B. and Hazen, R.M., 2022. Evidence for the oxidation of Earth's crust from the evolution of manganese minerals. Nature Communications, 13, 960.

Jiang, T., Yang, Y., Huang, Z., Zhang, B. and Qiu, G., 2004. Leaching kinetics of pyrolusite from manganese–silver ores in the presence of hydrogen peroxide. Hydrometallurgy, 72, 129-138.

Jiang, X.D., Zhao, X., Chou, Y.M., Liu, Q.S., Roberts, A.P., Ren, J.B., Sun, X.M., Li, J.H., Tang, X., Zhao, X.Y. and Wang, C.C., 2020. Characterization and quantification of magnetofossils within abyssal manganese nodules from the Western Pacific Ocean and implications for nodule formation. Geochemistry, Geophysics, Geosystems, 21, e2019GC008811

Johnson, J.E., Webb, S.M., Thomas, K., Ono, S., Kirschvink, J.L. and Fischer, W.W., 2013. Manganese-oxidizing photosynthesis before the rise of cyanobacteria. Proceedings of the National Academy of Sciences, 110, 11238-11243.

Jung, H., Chadha, T.S., Kim, D., Biswas, P. and Jun, Y.-S., 2017. Photochemically assisted fast abiotic oxidation of manganese and formation of δ-MnO_2 nanosheets in nitrate solution. Chemical Communications, 53, 4445-4448.

Kasten, S., Glasby, G.P., Schulz, H.D., Friedrich, G. and Andreev, S.I., 1998. Rare earth elements in manganese nodules from the South Atlantic Ocean as indicators of oceanic bottom water flow. Marine Geology, 146, 33-52.

Kasting, J.F., Schopf, J.W. and Klein, C., 1992. Models relating to Proterozoic atmospheric and oceanic chemistry. The Proterozoic Biosphere: A Multidisciplinary Study, 1185-1187.

Katsev, S., Rancourt, D.G. and L'Heureux, I., 2004. dSED: a database tool for modeling sediment early diagenesis. Computers and Geosciences, 30, 959-967.

Kendall, B., Reinhard, C.T., Lyons, T.W., Kaufman, A.J., Poulton, S.W. and Anbar, A.D., 2010. Pervasive oxygenation along late Archaean ocean margins. Nature Geoscience, 3, 647-652.

Khan, S., Maphalala, B., Nontso, Z., Magweregwede, F. and Godfrey, L., 2022. South Africa's resource availability as a driver for transitioning to a Circular Economy. Council for Scientific and Industrial Research Report Number: CSIR/MIN/MMR/IR/2022/0001/A. CSIR: Pretoria.

Killick, A.M., 2020. The setting and style of manganese mineralization in the Constantiaberg Massif, Cape Peninsula, South Africa. South African Journal of Geology 2020, 123, 493-510.

Kivinen, V., Krogerus, H. and Daavittila, J., 2010. Upgrading of Mn/Fe ratio of low-grade manganese ore for ferromanganese production. In The Twelfth International Ferro-Alloys Congress, Helsinki, Finland, 467-476.

Klein, C. and Beukes, N.J., 1993. Sedimentology and geochemistry of the late Proterozoic Rapitan Iron-Formation in Canada. Economic Geology, 88, 542-565.

Kleyenstüber, A.S.E., 1984. The mineralogy of the manganese-bearing Hotazel Formation of the Proterozoic Transvaal Sequence in Griqualand West, South Africa: Transactions of the Geological Society of South Africa, 87, 257-272.

Konhauser, K.O., 2007. Introduction to Geomicrobiology. Blackwell Publishing, Malden, USA, 425pp

Konhauser, K.O., Amskold, L.A., Lalonde, S.V., Posth, N., Kappler, A. and Anbar, A.D., 2007. Decoupling photochemical Fe (II) oxidation from shallow-water BIF deposition. Earth and Planetary Science Letters, 258, 87-100.

Konhauser, K.O., Hamade, T., Raiswell, R., Morris, R.C., Ferris, F.G., Southam, G. and Canfield, D.E., 2002. Could bacteria have formed the Precambrian banded iron formations? Geology, 30, 1079-1082.

Koplitz, L.V., Kim, K. and McClure, D.S., 1994. Temperature dependence of 10Dq for aqueous hexaaquomanganese (II). Inorganic Chemistry, 33, 702-704.

Kozak, M., 2019. Jupiter Mines Limited Equity Research Report. Cantor Fitzgerald, 33pp

Krogerus, H., Daavittila, J., Vehvilainen, J. and Honkaniemi, M., 2013. The application of steel belt technology for sintering of manganese ore fines. Proceeding of the 8th International Ferro-Alloys Congress, 271-278.

Kuleshov, V.N., 2012. A superlarge deposit–Kalahari manganese ore field (Northern Cape, South Africa): Geochemistry of isotopes ($\delta^{13}C$ and $\delta^{18}O$) and genesis. Lithology and Mineral Resources, 47, 217-233.

Kurzweil, F., Wille, M., Gantert, N., Beukes, N.J. and Schoenberg, R., 2016. Manganese oxide shuttling in pre-GOE oceans-evidence from molybdenum and iron isotopes. Earth and Planetary Science Letters, 452, 69-78.

Laznicka, P., 1992. Manganese deposits in the global lithogenetic system: Quantitative approach. Ore Geology Reviews, 7, 279-356.

Lechte M. and Wallace M., 2016. Sub-ice shelf ironstone deposition during the Neoproterozoic Sturtian glaciation. Geology, 44, 891-894.

Lewis, B.L. and Landing, W.M., 1991. The biogeochemistry of manganese and iron in the Black Sea. Deep Sea Research Part A. Oceanographic Research Papers, 38, S773-S803.

Li, Y., Huang, Y., Wu, W., Yan, M. and Xie, Y., 2021. Research and application of arsenic-contaminated groundwater remediation by manganese ore permeable reactive barrier. Environmental Technology, 42, 2009-2020.

Lishchuk, V., Koch, P. H., Lund, C. and Lamberg, P., 2015. The geometallurgical framework. Malmberget and Mikheevskoye case studies. Mining Science, 22, 57-66.

Liu, W., Hao, J., Elzinga, E.J., Piotrowiak, P., Nanda, V., Yee, N. and Falkowski, P.G., 2020. Anoxic photogeochemical oxidation of manganese carbonate yields manganese oxide. Proceedings of the National Academy of Sciences, 117, 22698-22704. doi: 10.1073/pnas.2002175117

Long, Y., Pan, J., Farooq, S. and Boer, H., 2016. A sustainability assessment system for Chinese iron and steel firms. Journal of Cleaner Production, 125, 133-144.

Lovley, D.R., 1991. Dissimilatory Fe(III) and Mn(IV) reduction. Microbiological Reviews, 55, 259-287.

Lüders, V., Gutzmer, J. and Beukes, N.J., 1999. Fluid inclusion studies in cogenetic hematite, hausmannite, and gangue minerals from high-grade manganese ores in the Kalahari manganese field, South Africa. Economic Geology, 94, 589-595.

Lund, C., 2013. Mineralogical, chemical and textural characterisation of the

Malmberget iron ore deposit for a geometallurgical model. Unpublished Ph.D. thesis, Luleå Tekniska Universitet, Sweden, 100pp

Lund, C. and Lamberg, P., 2014. Geometallurgy–a tool for better resource efficiency. European Geologist, 37, 39-43.

Luo, G., Ono, S., Beukes, N.J., Wang, D.T., Xie, S. and Summons, R.E., 2016. Rapid oxygenation of Earth's atmosphere 2.33 billion years ago. Science Advances, 2, e1600134.

Lyons, T.W., Diamond, C.W. and Konhauser, K.O., 2020. Shedding light on manganese cycling in the early oceans. Proceedings of the National Academy of Sciences, 117, 25960-25962.

MacGregor, D.G., 2013. Manganese deposits of the Cape Peninsula, South Africa. Unpublished M.Sc. thesis, University of Cape Town, South Africa, 139pp

Machamer, J.F., 1987. Working classification of manganese deposits. Mining Magazine, 157, 348-51.

Madison, A.S., Tebo, B.M., Mucci, A., Sundby, B. and Luther, G.W., 2013. Abundant porewater Mn (III) is a major component of the sedimentary redox system. Science, 341, 875-878. doi: 10.1126/science.1241396

Marchant, J.W., Willis, J.P. and Duncan, A.R., 1978. Geochemistry of the Table Mountain Group, I: Aspects of the origin of the Houtbaai manganese deposit. South African Journal of Geology, 81, 179-184.

Markgraaff, J., 2019. Ore variability management at Mamatwan manganese mine for an improved sinter product. Unpublished M.Eng. thesis, North-West University, South Africa, 168pp

Mayanna, S., Peacock, C.L., Schäffner, F., Grawunder, A., Merten, D., Kothe, E. and Büchel, G., 2015. Biogenic precipitation of manganese oxides and enrichment of heavy metals at acidic soil pH. Chemical Geology, 402, 6-17.

Maynard, J.B., 2003. Manganiferous sediments, rocks, and ores. Treatise on Geochemistry, 7, 407. doi:10.1016/B0-08-043751-6/07099-7

Maynard, J.B., 2010. The chemistry of manganese ores through time: A signal of increasing diversity of Earth-surface environments. Economic Geology 105, 535-552. doi: 10.2113/gsecongeo.105.3.535.

McClung, C.R. and Viljoen, F., 2011. A detailed mineralogical assessment of sphalerites from the Gamsberg zinc deposit, South Africa: The manganese conundrum. Minerals Engineering, 24, 930-938.

McNulty, B.A. and Jowitt, S.M., 2021. Barriers to and uncertainties in understanding and quantifying global critical mineral and element supply. iScience, 24, 102809.

Mhlanga, X.R., Tsikos, H., Lee, B., Rouxel, O.J., Boyce, A.C., Harris, C. and Lyons, T.W., 2023. The Palaeoproterozoic Hotazel BIF-Mn Formation as an archive of Earth's earliest oxygenation. Earth Science Reviews 240, 104389.

Miyano, T. and Beukes, N.J., 1987. Physicochemical environments for the formation of quartz-free manganese oxide ores from the early Proterozoic Hotazel Formation, Kalahari manganese field, South Africa. Economic Geology, 82, 706-718.

Moore, J.M., Kuhn, B.K., Mark, D.F. and Tsikos, H., 2012. A sugilite-bearing assemblage from the Wolhaarkop breccia, Bruce iron-ore mine, South Africa: evidence for alkali metasomatism and ^{40}Ar–^{39}Ar dating. European Journal of Mineralogy, 24, 773-773

Morgan, J.J., 2005. Kinetics of reaction between O_2 and Mn(II) species in aqueous solutions. Geochimica et Cosmochimica Acta, 69, 35-48.

Motloba, G.B., Viljoen, K.S., Rose, D.H. and Smith, A.J.B., 2024. The processing behaviour of the sphalerites from the Big Syncline deposit, South Africa. South African Journal of Geology, 127, 71-94.

Mpho, M., Samson, B. and Ayo, A., 2013. Evaluation of reduction roasting and magnetic separation for upgrading Mn/Fe ratio of fine ferromanganese. International Journal of Mining Science and Technology, 23, 537-541.

Murray, J.W., Dillard, J.G., Giovanoli, R., Mores, H. and Stumm, W., 1985. Oxidation of Mn(II): initial mineralogy, oxidation state and ageing. Geochimica et Cosmochimica Acta, 49, 463-470. doi:10.1016/0016-7037(85)90038-9

Murthy, B.V.S., Madhusudan Rao, B., Dubey, A.K. and Srinivasulu, 2009. Geophysical exploration for manganese-some first-hand examples from Keonjhar district, Orissa. Journal of Indian Geophysical Union, 13, 149-161.

Myers, C.R. and Nealson, K.H., 1988. Bacterial manganese reduction and growth with manganese oxide as the sole electron acceptor. Science, 240, 1319-1321.

Namgung, S., Chon, C.M. and Lee, H., 2018. Formation of diverse Mn oxides: a review of biogeochemical processes of Mn oxidation. Geosciences, 22, 373-381. doi:10.1007/s12303-018-0002-7

Naseri, T., Pourhossein, F., Mousavi, S.M., Kaksonen, A.H. and Kuchta, K., 2022. Manganese bioleaching: an emerging approach for manganese recovery from spent batteries. Reviews in Environmental Science and Bio/Technology, 21, 447-468.

Nayl, A.A., Ismail, I.M. and Aly, H.F., 2011. Recovery of pure $MnSO_4 \cdot H_2O$ by reductive leaching of manganese from pyrolusite ore by sulfuric acid and hydrogen peroxide. International Journal of Mineral Processing, 100, 116-123.

Nel, C.J., Beukes, N.J. and De Villiers, J.P,B., 1986. The Mamatwan manganese mine of the Kalahari manganese field. In: C.B. Anhaeuser and S. Maske (Editors), Mineral Deposits of Southern Africa. Geological Society of South Africa, Johannesburg, 963-978.

Newton, A.G. and Kwon, K.D., 2020. Classical mechanical simulations of layer- and tunnel-structured manganese oxide minerals. Geochimica et Cosmochimica Acta, 291, 92-109.

O'shaughnessy, P., Kim, J.K. and Lee, B.W., 2004. The smelting of manganese carbonate ore. Proceedings of the Tenth International Ferro-Alloys Congress, 1, 1-4.

Ogungbuyi, P.I., Janney, P.E. and Harris, C., 2022. Carbonatite, aillikite and olivine melilitite from Zandkopsdrift, Namaqualand, South Africa: Constraints on the origin of an unusual lamprophyre-dominated carbonatite complex and the nature of its mantle source. Lithos, 418, 106678.

Olson, S.L., Kump, L.R. and Kasting, J.F., 2013. Quantifying the areal extent and dissolved oxygen concentrations of Archean oxygen oases. Chemical Geology, 362, 35-43.

Oonk, P.B.H., Tsikos, H., Mason, P.R.D., Henkel, S., Staubwasser, M., Fryer, L., Poulton, S.W. and Williams, H.M., 2017. Fraction-specific controls on the trace element distribution in iron formations: Implications for trace metal stable isotope proxies. Chemical Geology, 474, 17-32.

Ortiz, J. M., 2019. Geometallurgical modeling framework. Predictive Geometallurgy and Geostatistics Lab Annual Report, Queens University, Canada. 178pp

Ortlepp, R.J., 1964. Nsutite (battery grade manganese dioxide) from the Western Transvaal. Transactions of the Geological Society of South Africa, 67, 149-161.

Ossa Ossa, F., Hofmann, A., Vidal, O., Kramers, J.D., Belyanin, G. and Cavalazzi, B., 2016. Unusual manganese enrichment in the Mesoarchean Mozaan Group, Pongola Supergroup, South Africa. Precambrian Research, 281, 414-433.

Ovechkina, M.N., Watkeys, M.K., Mostovski, M.B., Kretzinger, W. and Perritt, S.M., 2021. Calcareous nannofossils identify the age and precipitation rates of manganese deposits of the Mozambique Ridge and Mozambique Basin, SW Indian Ocean. Geo-Marine Letters, 41, 1-14.

Pack, A., Gutzmer, J., Beukes, N.J., Van Niekerk, H.S. and Hoernes, S., 2000. Supergene ferromanganese wad deposits derived from Permian Karoo Strata along the late cretaceous–mid-tertiary African Land Surface, Ryedale, South Africa. Economic Geology, 95, 203-220.

Partridge, T.C. and Maud, R.R., 1987. Geomorphic evolution of southern Africa since the Mesozoic. South African Journal of Geology, 90, 179-208.

Peterson, M.J., Manuel, J.R. and Hapugoda, S., 2021. Geometallurgical characterisation of Mn ores. Applied Earth Science, 130, 2-22.

Pharoe, B.K., Evdokimov, A.N., Gembitskaya, I.M. and Bushuyev, Y.Y., 2020. Mineralogy, geochemistry and genesis of the post-Gondwana supergene manganese deposit of the Carletonville-Ventersdorp area, North West Province, South Africa. Ore Geology Reviews, 120, 103372. doi: 10.1016/j.oregeorev.2020.103372

Pharoe, B.K. and Liu, K., 2018. Stratigraphy of the pedogenic manganese nodules in the Carletonville area, North West Province of South Africa: A case study of the General Nice Manganese Mine. Journal of African Earth Sciences, 143, 79-101.

Pienaar, P.C. and Smith, W.F.P., 1992. A case study of the production of high-grade manganese sinter from low-grade Mamatwan manganese ore.

Proceedings of the 6th International Ferro-Alloys Congress, 1, 131-138.

Planavsky, N., Asael, D., Hofmann, A., Reinhard, C.T., Lalonde, S.V., Knudsen, A., Wang, X., Ossa Ossa, F., Pecoits, E., Smith, A.J.B., Beukes, N.J., Bekker, A., Johnson, T.M., Konhauser, K.O., Lyons, T.W. and Rouxel, O.J., 2014. Evidence for oxygenic photosynthesis half a billion years before the Great Oxidation Event. Nature Geoscience, 7, 283-286.

Planavsky, N., Bekker, A., Rouxel, O.J., Kamber, B., Hofmann, A., Knudsen, A. and Lyons, T.W., 2010. Rare Earth Element and yttrium compositions of Archean and Paleoproterozoic Fe formations revisited: New perspectives on the significance and mechanisms of deposition. Geochimica et Cosmochimica Acta, 74, 6387-6405.

Planavsky, N., Rouxel, O., Bekker, A., Shapiro, R., Fralick, P. and Knudsen, A., 2009. Iron-oxidizing microbial ecosystems thrived in late Paleoproterozoic redox-stratified oceans. Earth and Planetary Science Letters, 286, 230-242.

Pochart, G., Joncourt, L., Touchard, N. and Perdon, C., 2007. Metallurgical benefit of reactive high-grade ore in manganese alloys manufacturing. World, 800, 1200.

Post, J.E., 1999. Manganese oxide minerals: Crystal structures and economic and environmental significance. Proceedings of the National Academy of Sciences, 96, 3447-3454.

Poulton, S.W., Bekker, A., Cumming, V.M., Zerkle, A.L., Canfield, D.E. and Johnston, D.T., 2021. A 200-million-year delay in permanent atmospheric oxygenation. Nature, 592, 232-236.

Preston, P.C.C.R., 2001. Physical and chemical characterization of the manganese ore bed at the Mamatwan mine, Kalahari Manganese Field. Unpublished M.Sc. thesis, University of Johannesburg, South Africa. 146pp

Ramazi, H. and Mostafaie, K., 2013. Application of integrated geoelectrical methods in Marand (Iran) manganese deposit exploration. Arabian Journal of Geosciences, 6, 2961-2970.

Renno, A.D., Le Bras, L., Ziegenrücker, R., Couffignal, F., Wiedenbeck, M., Haser, S. and Hlawacek, G., 2016. In detail monazite characterization in a carbonatite weathering profile-a new tool for landscape geochronology. In American Geophysical Union Fall Meeting Abstracts V23A-2966.

Robbins, L.J., Fakhraee, M., Smith, A.J.B., Bishop, B.A., Swanner, E.D., Peacock, C.L., Wang, C.-L., Planavsky, N.J., Reinhard, C.T., Crowe, S.A. and Lyons, T.W., 2023. Manganese oxides, Earth surface oxygenation, and the rise of oxygenic photosynthesis. Earth-Science Reviews, 239, 104368.

Rogers, J., 1995. A comparative study of manganese nodules off southern Africa. South African Journal of Geology, 98, 208-216.

Roy, S., 1988. Manganese metallogenesis: a review. Ore Geology Reviews, 4, 155-170.

Roy, S., 1997. Genetic diversity of manganese deposition in the terrestrial geological record. Geological Society, London, Special Publications, 119, 5-27.

Rozendaal, A., Rudnick, T.K. and Heyn, R., 2017. Mesoproterozoic base metal sulphide deposits in the Namaqua sector of the Namaqua-Natal Metamorphic Province, South Africa: a review. South African Journal of Geology, 120, 153-186.

Schaefer, M.O., Gutzmer, J. and Beukes, N.J., 2001. Late Paleoproterozoic Mn-rich oncoids: Earliest evidence for microbially mediated Mn precipitation. Geology, 29, 835-838.

Schier, K., Bau, M., Smith, A.J.B., Beukes, N.J., Coetzee, L.L. and Viehmann, S., 2020. Chemical evolution of seawater in the Transvaal Ocean between 2426 Ma (Ongeluk Large Igneous Province) and 2413 Ga (Kalahari Manganese Field) ago. Gondwana Research, 88, 373-388.

Schippers, A., Neretin, L.N., Lavik, G., Leipe, T. and Pollehne, F., 2005. Manganese(II) oxidation driven by lateral oxygen intrusions in the western Black Sea. Geochimica et Cosmochimica Acta, 69, 2241-2252.

Schouwstra, R., De Vaux, D., Hey, P., Malysiak, V., Shackleton, N. and Bramdeo, S., 2010. Understanding Gamsberg–A geometallurgical study of a large stratiform zinc deposit. Minerals Engineering, 23, 960-967.

Schneiderhahn, E.A., Gutzmer, J., Strauss, H., Mezger, K. and Beukes, N.J. 2006. The chemo-stratigraphy of a Paleoproterozoic MnF-BIF succession – the Voëlwater Subgroup of the Transvaal Supergroup in Griqualand West, South Africa. South African Journal of Geology, 109, 63-80.

Schröder, S., Bedorf, D., Beukes, N.J. and Gutzmer, J., 2011. From BIF to red beds: Sedimentology and sequence stratigraphy of the Paleoproterozoic Koegas Subgroup (South Africa). Sedimentary Geology, 236, 25-44.

Siahi, M., Tsikos, H., Rafuza, S., Oonk, P.B.H., Mason, P.R.D., Mhlanga, X.R., van Niekerk, D. and Harris, C., 2020. Insights into the processes and controls for the absolute abundance and distribution of manganese in Precambrian Iron Formations. Precambrian. Research, 350, 105878.

Singh, V., Chakraborty, T. and Tripathy, S.K., 2020. A review of low grade manganese ore upgradation processes. Mineral Processing and Extractive Metallurgy Review, 41, 417-438.

Sinha, M.K. and Purcell, W., 2019. Reducing agents in the leaching of manganese ores: A comprehensive review. Hydrometallurgy, 187, 168-186.

Smith, A.J.B., 2015. The life and times of banded iron formations. Geology, 43, 1111-1112.

Smith, A.J.B., 2018. The Iron Formations of Southern Africa. In: S. Siegesmund, M.A.S. Basei, P. Oyhantçabal and S. Oriolo (Editors), Geology of Southwest Gondwana. Springer, Cham, 469-491.

Smith, A.J.B. and Beukes, N.J., 2016. Palaeoproterozoic banded iron formation-hosted high-grade hematite iron ore deposits of the Transvaal Supergroup, South Africa. Episodes, 39, 269-284.

Smith, A.J.B., Beukes, N.J., Gutzmer, J., Czaja, A.D., Johnson, C.M. and Nhleko, N., 2017. Oncoidal granular iron formation in the Mesoarchaean Pongola Supergroup, southern Africa: Textural and geochemical evidence for biological activity during iron deposition. Geobiology, 15, 731-749.

Smith, A.J.B. and Beukes, N.J., 2023. The paleoenvironmental implications of pre-Great Oxidation Event manganese deposition in the Mesoarchean Ijzermijn Iron Formation Bed, Mozaan Group, Pongola Supergroup, South Africa. Precambrian Research, 384, 106922.

Smith, A.J.B., Beukes, N.J., Cochrane, J. and Gutzmer, J., 2023. Manganese carbonate-bearing mudstone of the Witwatersrand-Mozaan succession in southern Africa as evidence for bacterial manganese respiration and availability of free molecular oxygen in Mesoarchaean oceans. South African Journal of Geology, 126, 29-48.

Smrzka, D., Zwicker, J., Bach, W., Feng, D., Himmler, T., Chen, D. and Peckmann, J., 2019. The behavior of trace elements in seawater, sedimentary pore water, and their incorporation into carbonate minerals: a review. Facies, 65, 1-47.

Srigutomo, W. and Pratomo, P.M., 2016. 2D resistivity and induced polarization measurement for manganese ore exploration. Journal of Physics: Conference Series, 739, 012138.

Steenkamp, J.D. and Basson, J., 2013, The manganese ferroalloys industry in southern Africa. The Journal of The Southern African Institute of Mining and Metallurgy, 113, 667-676.

Steenkamp, J.D., Bam, W.G., Ringdalen, E., Mushwana, M., Hockaday, S.A.C. and Sithole, N.A., 2018. Working towards an increase in manganese ferroalloy production in South Africa-a research agenda. Journal of the Southern African Institute of Mining and Metallurgy, 118, 645-654.

Steenkamp, J.D., Chetty, D., Singh, A., Hockaday, S.A.C. and Denton, G.M., 2020. From ore body to high temperature processing of complex ores: manganese – a South African perspective. Journal of The Minerals, Metals & Materials Society (JOM), 72, 3422-3435.

Strydom, D. and Visser, J.N.J., 1986. Nappe structures in the highly deformed Proterozoic metasedimentary Aggeneys-type sequence of western Bushmanland, South Africa. Precambrian Research, 33, 171-187.

Stumm, W. and Morgan, J.J., 1995. Aquatic Chemistry: Chemical Equilibria and Rates in Natural Waters, 3rd Edition. John Wiley, New York. 1040pp

Summerhayes, C.P. and Willis, J.P., 1975. Geochemistry of manganese deposits in relation to environment on the sea floor around southern Africa. Marine Geology, 18, 159-173.

Sundqvist, S., Khalilian, N., Leion, H., Mattisson, T. and Lyngfelt, A., 2017. Manganese ores as oxygen carriers for chemical-looping combustion (CLC) and chemical-looping with oxygen uncoupling (CLOU). Journal of Environmental Chemical Engineering, 5, 2552-2563.

Tathavadkar, V., Singh, V., Mishra, P.K., Mallick, P. and Nanda, B.D., 2010. Effect of manganese ore blends on performance of submerged arc furnace for ferromanganese production. Ironmaking & Steelmaking, 37, 103-111.

Tebo M.B., Nealson K.H., Emerson S. and Jacobs L., 1984. Microbial mediation of Mn(II) and Co(II) precipitation at the O_2/H_2S interfaces in two anoxic fjords. Limnology and Oceanography, 29, 1247-1258.

Tebo, B. M., 1991. Manganese(II) oxidation in the suboxic zone of the Black Sea. Deep-Sea Research, 38, S883-S905.

Tebo, B.M., Bargar, J.R., Clement, B.G., Dick, G.J., Murray, K.J., Parker, D., Verity, R. and Webb, S.M., 2004. Biogenic manganese oxides: Properties and mechanisms of formation. Annual Reviews in Earth and Planetary Sciences, 32, 287-328.

Tebo, B.M., Johnson, H.A., McCarthy, J.K. and Templeton, A.S., 2005. Geomicrobiology of manganese(II) oxidation. Trends in Microbiology, 13, 421-428.

Thomazo, C. and Papineau, D., 2013. Biogeochemical cycling of nitrogen on the early Earth. Elements, 9, 345-351.

Tian, Y., Etschmann, B., Mei, Y., Grundler, P.V., Testemale, D., Hazemann, J.L., Elliott, P., Ngothai, Y. and Brugger, J., 2014. Speciation and thermodynamic properties of manganese (II) chloride complexes in hydrothermal fluids: in situ XAS study. Geochimica et Cosmochimica Acta, 129, 77-95.

Trouwborst, R.E., Clement, B.G., Tebo, B.M., Glazer, B.T. and Luther, G.W., 2006. Soluble Mn (III) in suboxic zones. Science, 313, 1955-1957. doi: 10.1126/science.113287

Tsikos, H., Beukes, N.J., Moore, J.M. and Harris, C., 2003. Deposition, diagenesis, and secondary enrichment of metals in the Paleoproterozoic Hotazel Iron Formation, Kalahari Manganese Field, South Africa. Economic Geology, 98, 1449-1462.

Tsikos, H., Matthews, A., Erel, Y. and Moore, J.M., 2010. Iron isotopes constrain biogeochemical cycling of Fe and Mn in a Palaeoproterozoic stratified basin. Earth & Planetary Science Letters, 298, 125-134.

Tsikos, H. and Moore, J.M., 1997. Petrography and geochemistry of the Palaeoproterozoic Hotazel iron-formation, Kalahari Manganese Field, South Africa: Implications for Precambrian manganese metallogenesis. Economic Geology, 92, 87-97.

U.S. Geological Survey, 2024. Mineral commodity summaries 2024: U.S. Geological Survey, 212pp, https://doi.org/10.3133/mcs2024

Vafeas, N.A., Blignaut, L.C., Viljoen, K.S. and Meffre, S., 2018. New evidence for the early onset of supergene alteration along the Kalahari unconformity. South African Journal of Geology, 121, 157-170.

Vafeas, N.A., Viljoen, K.S. and Blignaut, L.C., 2019. Mineralogical characterization of the thrusted manganese ore above the Blackridge Thrust Fault, Kalahari Manganese Field: The footprint of the Mukulu Enrichment. Island Arc, 28, 12280.

Van Cappellen, P.V., Viollier, E., Roychoudhury, A., Clark, L., Ingall, E., Lowe, K. and Dichristina, T., 1998. Biogeochemical Cycles of Manganese and Iron at the Oxic–Anoxic Transition of a Stratified Marine Basin (Orca Basin, Gulf of Mexico). Environmental Science and Technology 32, 2931-2939.

Van Niekerk, H.S., 2006. The origin of the Kheis Terrane and its relationship with the Archean Kaapvaal Craton and the Grenvillian Namaqua Province in southern Africa. Unpublished Ph.D. thesis, University of Johannesburg, South Africa, 402pp

Van Niekerk, H.S., Beukes, N.J. and Gutzmer, J., 1999. Post-Gondwana pedogenic ferromanganese deposits, ancient soil profiles, African land surfaces and palaeoclimatic change on the Highveld of South Africa. Journal of African Earth Sciences, 29, 761-781.

Verlaan, P.A. and Cronan, D.S., 2022. Origin and variability of resource-grade marine ferromanganese nodules and crusts in the Pacific Ocean: A review of biogeochemical and physical controls. Geochemistry, 82, 125741.

Veizer, J., Hoefs, J., Lowe, D.R. and Thurston, P.C., 1989. Geochemistry of Precambrian carbonates: II. Archean greenstone belts and Archean sea water. Geochimica et Cosmochimica Acta, 53, 859-871.

Visser, M., Smith, H., Ringdalen, E. and Tangstad, M., 2013. Properties of Nchwaning and Gloria ore in the production of Mn ferro-alloys. In Proceedings of the 13th International Ferro-Alloys Congress, 553-566.

Von der Heyden, B.P., La Cock, R.A., Ferreira, D.R., Conradie, T.A., van Rooyen, J. and Palcsu, L., 2024. Mineralisation controls for the diverse Cape manganese occurrences, South Africa. South African Journal of Geology, 127, 619-640.

von Plehwe-Leisen, E. and Klemm, D.D., 1995. Geology and ore genesis of the manganese ore deposits of the Postmasburg manganese-field, South Africa. Mineralium Deposita, 30, 257-267.

Webb, S.M., Tebo, B.M. and Bargar, J.R., 2005. Structural characterization of biogenic Mn oxides produced in seawater by the marine Bacillus sp. strain SG-1. American Mineralogist, 90, 1342-1357.

Westfall, L.A., Davourie, J., Ali, M. and McGough, D., 2016. Cradle-to-gate life cycle assessment of global manganese alloy production. The International Journal of Life Cycle Assessment, 21, 1573-1579.

Williams, T.M. and Owen, R.B., 1990. Authigenesis of ferric oolites in superficial sediments from Lake Malawi, Central Africa. Chemical geology, 89, 179-188.

Willis, J.P. and Ahrens, L.H., 1962. Some investigations on the composition of manganese nodules, with particular reference to certain trace elements. Geochimica et Cosmochimica Acta, 26, 751-764.

World Steel in Figures, 2023 edition. 7 June 2023, World Steel Association, https://worldsteel.org/steel-topics/statistics/world-steel-in-figures-2023/

Yan, H., Pi, D.H., Jiang, S.Y., Mao, J., Xu, L., Yang, X., Hao, W., Mänd, K., Li, L., Konhauser, K.O. and Robbins, L.J., 2022. Mineral paragenesis in Paleozoic manganese ore deposits: Depositional versus post-depositional formation processes. Geochimica et Cosmochimica Acta, 325, 6586.

Zhang, W. and Cheng, C.Y., 2007. Manganese metallurgy review. Part I: Leaching of ores/secondary materials and recovery of electrolytic/chemical manganese dioxide. Hydrometallurgy, 89, 137-159.

Ziemann, S., Grunwald, A., Schebek, L., Müller, D.B. and Weil, M., 2013. The future of mobility and its critical raw materials. Metallurgical Research & Technology, 110, 47-54.

Editorial handling: M.A. Elburg.